

Profile Monitoring via Eigenvector Perturbation

Takayuki Iguchi*

Department of Statistics, Florida State University
and

Andrés F. Barrientos

Department of Statistics, Florida State University
and

Eric Chicken

Department of Statistics, Florida State University
and

Debajyoti Sinha

Department of Statistics, Florida State University

November 6, 2024

Abstract

In Statistical Process Control, control charts are often used to detect undesirable behavior of sequentially observed quality characteristics. Designing a control chart with desirably low False Alarm Rate (FAR) and detection delay (ARL_1) is an important challenge especially when the sampling rate is high and the control chart has an In-Control Average Run Length, called ARL_0 , of 200 or more, as commonly found in practice. Unfortunately, arbitrary reduction of the FAR typically increases the ARL_1 . Motivated by eigenvector perturbation theory, we propose the Eigenvector Perturbation Control Chart for computationally fast nonparametric profile monitoring. Our simulation studies show that it outperforms the competition and achieves both $ARL_1 \approx 1$ and $ARL_0 > 10^6$.

Keywords: Statistical Process Control, Nonparametric Profile Monitoring, Change-point Detection, Alarm Fatigue, False Alarm Rate (FAR)

*T. Iguchi is Assistant Professor, Air Force Institute of Technology. The work was part of his PhD dissertation at Florida State University. This research was supported by the Office of the Secretary of Defense, Directorate of Operational Test and Evaluation under Grant FA8075-14-D-0019 and the Test Resource Management Center under the Science of Test research program grant FA807518F1525. The views expressed in this article are those of the author and do not reflect the official policy or position of the United States Air Force, Department of Defense, or the U.S. Government. This article has been accepted for publication in *Technometrics*, published by Taylor & Francis.

1 Introduction

The main objective of statistical process control (SPC) is to monitor whether a process of interest generating observed quality characteristics is changing over time. Our particular SPC context focuses on designing methods to monitor profiles of quality characteristics. These profile monitoring methods have found applications in manufacturing processes, crime monitoring, and monitoring objects' locations via wireless technology. For examples, see the review in Maleki, Amiri, and Castagliola (2018) and the references therein. The assumptions about the stochastic models generating the profiles are pivotal in the development of the SPC monitoring methods, usually called control charts. Increasing complexities of processes of interest due to rapid technological developments and automated data acquisition drive the need for more widely applicable and easily implementable control charts. Control charts find use in diverse fields, including public health surveillance (Bersimis and Sachlas 2022), stamping operation force monitoring (Jin and Shi 1999), artificial sweetener manufacturing (Kang and Albin 2000), mechanical component manufacturing (Colosimo, Semeraro, and Pacella 2008), and automobile engineering (Amiri, Jensen, and Kazemzadeh 2009).

Two main challenges exist in control chart design: lowering the False Alarm Rate (FAR) when the underlying process is in-control (IC) (i.e., desirable), and reducing the detection delay after the underlying process becomes out-of-control (OOC) (i.e., undesirable). Negative consequences of a high number of false alarms include an increased cost due to unwarranted disruption caused by each false alarm and a loss of user's confidence in alarms. For example, in hospital intensive care units, the FAR has detrimental effects on patient safety and effectiveness of care (Imhoff and Kuhls 2006). These problems are only exacerbated as the time interval between two consecutive monitoring times decreases, a frequent event with streaming data (Woodall and Faltin 2019). Often, control charts are calibrated to ensure that an average number of monitoring times needed to observe the next false alarm under an IC process, called the IC Average Run Length (ARL_0), is 200. If a process is monitored each millisecond, the average time to a false alarm under this level of calibration of ARL_0 would be 200 milliseconds, which is clearly undesirable. Widening of control limits may increase the ARL_0 , but typically comes at the cost of delayed detection of an OOC process.

In this paper, our goal is to provide an easily implementable nonparametric control chart applicable to a wide variety of quality characteristics, when the observed quality characteristics $\mathbf{y}^t = (y_1^t, \dots, y_n^t)$ at discrete monitoring time-point t are noisy observations of the scalar function $f^t : \mathbb{R}^d \rightarrow \mathbb{R}$ evaluated at n sampled values $\mathbf{x}_1^t, \dots, \mathbf{x}_n^t$ of a random vector of d explanatory variables. So, the observed y_i^t of each functional profile has mean $\mathbb{E}[Y_i^t | \mathbf{x}_i^t] = f^t(\mathbf{x}_i^t)$. Our goal is to achieve a low FAR and a high ARL_0 without sacrificing low detection delay. To achieve these goals, our method leverages the $(w \times w)$ sample correlation matrix \mathbf{R} of the profiles $\mathbf{y}^{t-w+1}, \dots, \mathbf{y}^t$ across $w > 1$ monitoring times (including the current as well as past $w - 1$), with the (s, r) -th entry of \mathbf{R} being $R_{s,r} = \frac{\sum_{i=1}^n (y_i^r - \bar{y}^r)(y_i^s - \bar{y}^s)}{\sqrt{\sum_{i=1}^n (y_i^r - \bar{y}^r)^2 \sum_{j=1}^n (y_j^s - \bar{y}^s)^2}}$ for $(t - w + 1) \leq s, r \leq t$, where $\bar{y}^r = \frac{1}{n} \sum_{i=1}^n y_i^r$. Essentially, \mathbf{R} is a consistent estimator of the the population correlation matrix $\mathbf{\Gamma}$ whose (r, s) -th element is derived from $\text{Cov}[Y^r, Y^s] = \mathbb{E}[\text{Cov}[Y^r, Y^s | \mathbf{x}^r, \mathbf{x}^s]] + \text{Cov}[\mathbb{E}[Y^r | \mathbf{x}^r], \mathbb{E}[Y^s | \mathbf{x}^s]]$, where the covariances and expectations are computed using the conditional distribution of $(Y^r, Y^s) | \mathbf{x}^r, \mathbf{x}^s$ and then the marginal distribution of $(\mathbf{x}^r, \mathbf{x}^s)$.

For the sake of brevity, our notations suppress the obvious dependence of \mathbf{R} on t and dimension w . To propose our control chart, we use the *structural* difference in \mathbf{R} computed from IC profiles when $f^{t-w+1} = \dots = f^t$ and the \mathbf{R} computed from mixture of IC and OOC profiles when $f^k \neq f^{k+1}$ for some $t - w < k < t$. Our proposed method exploits two ideas:

- A structural difference exists in $\mathbf{\Gamma}$ between the case when all w profiles are IC versus when the w profiles are a mix of IC and OOC. In the first case, $\mathbf{\Gamma}$ has a leading eigenvector $\frac{1}{\sqrt{w}}\mathbf{1}$. In the latter case, $\mathbf{\Gamma}$ has a four block structure (ignoring the diagonal) with its leading eigenvector being different from $\frac{1}{\sqrt{w}}\mathbf{1}$.
- According to recent work on Eigenvector Perturbation (EP), the distance between the observed normalized leading eigenvector \mathbf{v}_1 of a sample correlation matrix \mathbf{R} and the normalized leading eigenvector $\tilde{\mathbf{v}}_1$ of the population correlation matrix $\mathbf{\Gamma}$ is very small in ℓ_2 norm (Morales-Jimenez, Johnstone, McKay, and Yang 2021).

As a consequence of the above two, if observed $\mathbf{y}^{t-w+1}, \dots, \mathbf{y}^t$ used to compute \mathbf{R} are all IC profiles, then $\|\mathbf{v}_1 - \frac{1}{\sqrt{w}}\mathbf{1}\|_2$ should be small. Whereas, when $t + w - 1 < \tau < t$ for τ being the last monitoring time when the process is IC, then $\|\mathbf{v}_1 - \frac{1}{\sqrt{w}}\mathbf{1}\|_2$ should be large because some (but, not all) of these w profiles used for computing \mathbf{R} are OOC. If $\|\mathbf{v}_1 - \frac{1}{\sqrt{w}}\mathbf{1}\|_2$ exceeds some control limit U , we claim at least one of the w observed profiles is OOC. Hence, our proposed control chart using this EP property needs very few assumptions about the distributions of the error/noise and the predictors \mathbf{x}_i^k . To determine a control limit for our control chart from an empirically useful approximation of the distribution of eigenvector perturbation under w IC profiles, we use a bootstrap approach using a sample of m historical profiles that are known to be generated from the IC process.

Our simulation studies demonstrate that our control chart achieves an ARL_0 larger than 10^6 under a very general class of models for the IC profiles. As expected, such a large ARL_0 results in a low FAR even when the change-point occurs long after monitoring has begun (e.g., after 10^4 observed IC profiles). Typically, a control chart with such a large ARL_0 is expected to suffer from a large detection delay. For the competitors of our control chart, we show that a small increase of ARL_0 from 200 to 370 results in noticeable increases in ARL_1 . As a consequence, the calibrating control limits of the control charts of our competitors to achieve $ARL_0 > 10^6$ result in undesirably large ARL_1 values. Surprisingly, our proposed control chart is able to immediately detect an OOC process (i.e., $ARL_1 = 1$) even while maintaining $ARL_0 > 10^6$. Moreover, the proposed control chart is computationally fast, especially when compared to its existing competition (using multiple predictors). The combination of the extremely large ARL_0 , small ARL_1 , and desirable computational speed allows this control chart to be applied to streaming data with good performance.

The paper is organized as follows. Section 2 provides a brief background on profile monitoring (especially in the nonlinear nonparametric case) and on EP theory. Section 3 constructs the EP control chart and provides our method for determining control limits. Section 4 covers the simulation study exhibiting the superiority of the EP control chart in specificity and sensitivity as compared to other nonparametric monitoring methods for nonlinear profiles. Section 4 also discusses situations in which the EP control chart may

not perform satisfactorily. Section 5 applies the EP control chart and a PCA based control chart on a real world dataset. We conclude with a discussion in Section 6.

2 Background

Here, we describe the relevant background and associated models of profile monitoring in section 2.1, and provide a brief introduction to EP in section 2.2.

2.1 Profile Monitoring

In this paper, the model of the observed n scalar quality characteristics (y_1^t, \dots, y_n^t) at each time-point t is

$$y_i^t = f^t(\mathbf{x}_i^t) + \epsilon_i^t \quad \text{for } i = 1, \dots, n, \quad (1)$$

where $\mathbf{x}_i^t \in \mathbb{R}^d$ is the random vector of d dimensional explanatory variables, $\boldsymbol{\epsilon}^t = (\epsilon_1^t, \dots, \epsilon_n^t)$ with $\mathbb{E}[\boldsymbol{\epsilon}^t] = \mathbf{0}$ and $\text{Var}[\boldsymbol{\epsilon}^t] = \sigma^2 \mathbf{I}_n$ is a vector of independent and identically distributed mean-zero random noises inherently associated with the observation process. Here \mathbf{I}_n denotes a $(n \times n)$ identity matrix. In this setting, we assume the random design matrices $\mathbf{X}^t = (\mathbf{x}_1^t, \dots, \mathbf{x}_n^t)^\top$ at discrete monitoring time-points t to be identically distributed, and independent of the vector of errors $\boldsymbol{\epsilon}^t = (\epsilon_1^t, \dots, \epsilon_n^t)^\top$. However, we allow the correlation between noises ϵ_i^r and ϵ_i^s at two time-points $r \neq s$ via $\text{Cov}[\epsilon_i^r, \epsilon_i^s] = \phi\sigma^2$ with $\phi \in (-1, 1)$. We require \mathbf{x}_i^r and \mathbf{x}_i^s to be dependent for $r \neq s$. For the remainder of the paper, by the abuse of notation, we denote $f(\mathbf{x}_i^t)$ to be the functional relationship for the IC profile, that is, $f^t = f$ if at time t the process is known to be IC.

Profile monitoring typically consists of two steps: Phase I and Phase II. The Phase I analysis aims to define a notion of expected set of observations under IC process using a retrospective analysis of available historical IC profiles $\{(\mathbf{y}^t, \mathbf{X}^t) : t = -(m-1), \dots, 0\}$ when the process is known to be in control with $f^0 = \dots = f^{-m+1} = f$. Using the relevant range of summary statistics for an IC process obtained from Phase I, the Phase II analysis aims to detect the unusual deviation from an IC process in an online fashion using observations $\{(y_i^j, \mathbf{x}_i^j) : i \in [n]; j = -m+1, \dots, 0, \dots, t\}$ of quality characteristics at each discrete time $t \geq 1$. Ideally, a good profile monitoring method should not wrongly claim any process to be OOC at time $t \geq 1$ if the underlying process is actually IC at that time t , that is when $t \leq \tau$, where τ (typically unknown in practice) is the last monitoring time when the process is IC. If the process is IC indefinitely ($\tau = \infty$), we measure how often false alarms occur with the mean/expected time until a false alarm, $ARL_0 = \mathbb{E}[T_0]$, also called the IC average run length, where T_0 is the random time-point when the process is erroneously declared as OOC even when the process is still IC. If $\tau < \infty$, we use the False Alarm Rate (FAR) which is the probability of the next alarm occurring being a false alarm where the monitoring scheme is reset after each false alarm (but τ remains fixed). Also, a good monitoring method should signal a process to be OOC at time $t > \tau$ soon after it becomes OOC at time $\tau + 1$. Thus, another criterion of the performance of a profile monitoring method is the expected/mean time-interval $ARL_1 = \mathbb{E}[T_1 - \tau]$ where $T_1 > \tau$ is the random discrete time-point when an OOC is detected. Typically, a control chart

used for monitoring determines a process at time t to be IC (or OOC) if the monitoring statistic computed using observed $\{(\mathbf{y}^j, \mathbf{X}^j)\}_{j=-m+1}^t$ at time t lies inside (or outside) of an interval of lower and upper control limits. Akin to traditional hypothesis testing where a rejection region is specified prior to the statistical inference to ensure a desired significance level of the testing, the control limits are calibrated to ensure a desired ARL_0 value prior to commencing any monitoring performed in Phase II.

For existing profile monitoring methods, the choice of monitoring statistics is usually based on a set of assumptions about the underlying stochastic model of the profile and the corresponding method for estimation of f^t in (1). Performance of the parametric approaches for estimating f^t depends on the assumptions about the parametric form of f^t and the error distribution of ϵ_i^t . Poor performance of such profile monitoring methods (including incorrect ARL_0) can occur if the parametric assumptions regarding any of these two modeling components turn out to be incorrect. Additionally, in practice, we may only have access to quality historical data at $t = -m + 1, \dots, 0$ under IC process, and may not have any information about the parametric models of the OOC profiles and of the functions f^t when $t > \tau$. To address these practical challenges, we present below a nonparametric profile monitoring method with a control chart that neither uses any parametric form of the possibly non-linear and unknown f^t nor assumes any parametric distribution of ϵ_i^t in (1).

There is extensive literature on nonparametric profile monitoring using a univariate (scalar) predictor (Zou, Tsung, and Wang 2008; Colosimo, Semeraro, and Pacella 2008; Qiu, Zou, and Wang 2010; McGinnity, Chicken, and Pignatiello 2015; Qiu, Zi, and Zou 2018). The existing literature on multivariate/vector predictors is less extensive, and they can be categorized by the estimation procedures for f^t , the choice of monitoring statistics, the calibration methods for control limits, and whether the predictors vary over time.

The methods of Hung, Tsai, Yang, Chuang, and Tseng (2012) and Li, Pan, and Liao (2019) use support-vector regression (SVR), but the former uses an estimated \hat{f}^t as the monitoring statistics along with a moving block bootstrap confidence region of f^t as the control limit, and the later uses the nonparametric monitoring statistics of Williams et al. (2007) based on the residuals along with a nonparametric EWMA control chart of Hackl and Ledolter (1991). Both approaches rely on the observed ranks of the monitoring statistics compared to a set of values based on historical data. Although robust to possible outliers, these methods may not have good power and low ARL_1 because their rank-based monitoring statistics do not effectively use the underlying model of (1).

As an alternative, the semiparametric method by Iguchi, Barrientos, Chicken, and Sinha (2021) uses an ℓ_2 -based statistic of the estimated index parameters of the Single-Index Model (SIM) (Kuchibhotla and Patra 2020) for (y_i^t, \mathbf{x}_i^t) . Although this SIM based approach ensures a competitive FAR and ARL_1 , estimating index parameters is computationally slow which poses a problem in control limit calibration via Monte Carlo.

Due to the sequential nature of the profile monitoring problem, calibrating to a desired ARL_0 needs a Monte Carlo evaluation of ARL_0 using simulations of random run length T_0 , where T_0 is the random time-point of encountering a false alarm. For example, if T_0 follows a geometric distribution with mean ARL_0 , then $\text{Var}[T_0] = O(ARL_0^2)$. Therefore, calibrating control limits to large ARL_0 (say $ARL_0 > 10^6$) through a Monte Carlo approach is infeasible. Such approaches (as taken by Iguchi et al. (2021) and Li et al. (2019)) are not

only computationally intensive but also require explicit knowledge of f making the calibration effort parametric even when the monitoring approach for Phase II is nonparametric.

None of these existing nonparametric and semiparametric methods simultaneously enjoy a large ARL_0 , a small ARL_1 , and fast computational speed. Our proposed Eigenvector Perturbation control chart enjoys all of these desirable properties for large classes of IC and OOC profiles and with minimal assumptions about the error distributions. Our monitoring scheme detailed in Section 3.2 avoids the Monte Carlo approach to obtain the control limit that also achieves a large ARL_0 via using a Bootstrap method. Our proposed method to calibrate control limits for the EP control chart is detailed in Section 3.3.

2.2 Eigenvector Perturbation

Monitoring eigenspaces is popular in the change-point detection and SPC literature. Principal component analysis (PCA) type methods have been explored by Colosimo and Pacella (2007); Viveros-Aguilera, Steiner, and MacKay (2014); Wang, Mei, and Paynabar (2018) and others. To the best of our knowledge, application of ℓ_2 distance based EP is new to the SPC literature. To define this EP more explicitly in a general context, let us express a square matrix $\mathbf{M} \in \mathbb{R}^{w \times w}$ as $\mathbf{M} = \widetilde{\mathbf{M}} + \mathbf{E}$, where $\widetilde{\mathbf{M}} \in \mathbb{R}^{w \times w}$ is fixed matrix and \mathbf{E} is some random perturbation matrix. Let \mathbf{v} and $\tilde{\mathbf{v}}$ respectively be the leading eigenvectors of \mathbf{M} and $\widetilde{\mathbf{M}}$ with corresponding eigenvalues λ and $\tilde{\lambda}$. The goal is to answer the question: “*Under certain assumptions about $\widetilde{\mathbf{M}}$ and \mathbf{E} , how ‘far’ can the j th leading eigenvector \mathbf{v}_j of \mathbf{M} be from the j th leading eigenvector $\tilde{\mathbf{v}}_j$ of $\widetilde{\mathbf{M}}$?*” To employ EP to profile monitoring, we must do two things: (1) choose \mathbf{M} appropriately to reflect IC conditions, and (2) set a control limit based on either the possible values of \mathbf{E} or a sample of EPs under IC conditions.

For the first task, we draw inspiration from the work of Morales-Jimenez et al. (2021) on asymptotics of the eigenvalues and eigenvectors of the sample correlation matrix \mathbf{M} under a special case of spiked covariance model. Although the profiles in this paper do not follow the specific model in Morales-Jimenez et al. (2021), the covariance matrix of the responses from w IC profiles in certain cases follow a spiked covariance model. For example, if $\mathbf{X}^r = \mathbf{X}^s$ for $r \neq s$, then $\text{Cov}[y^1, \dots, y^w] = \text{Var}[f(\mathbf{x})]\mathbf{J}_w + \sigma^2\mathbf{I}$ where $\text{Var}[f(\mathbf{x})]$ corresponds to the common distribution of the explanatory variables \mathbf{x}^t and \mathbf{J}_w is a $w \times w$ unit matrix. If $\text{Var}[f(\mathbf{x})] > \sigma^2$, then one dominant eigenvalue exists and all other eigenvalues are small and equal. Due to the similarity of the eigenspace of the correlation matrices in our context and in the context in Morales-Jimenez et al. (2021), we consider the ℓ_2 EP of the sample correlation matrix. We construct the EP control chart in Section 3.2.

We now discuss the background relevant to our second task of adopting EP for profile monitoring. For the needed control limit of the EP, the literature provides nonasymptotic bounds on how large this can be depending on the properties of $\widetilde{\mathbf{M}}$ and \mathbf{E} . An important example is the Davis-Kahan $\sin(\theta)$ Theorem (Davis and Kahan 1970) which gives an upper bound of $\sin(\theta)$ where θ is the angle between $\tilde{\mathbf{v}}_j$ and \mathbf{v}_j . Using some arguments from trigonometry, any bound of $\sin(\theta)$ can be turned into a bound on ℓ_2 perturbation $\|\tilde{\mathbf{v}}_j - \mathbf{v}_j\|_2$. In the past decade, there has been growing literature on improving these bounds on ℓ_2 and, more recently, ℓ_∞ distances (see Chen, Chi, Fan, Ma, et al. (2021) for a review).

If the aim is to only reduce the probability of false alarms, setting a control limit to one

of these bounds can achieve zero probability of false alarms. Unfortunately, this and other bounds from the EP literature are not tight enough to be useful as practical control limits as the resulting control limits will have either very low or no sensitivity. To construct our control limits in Section 3.2, we leverage the knowledge of the existence of a nonasymptotic bound for the EP and the usually small perturbation of a sample correlation matrix.

3 Methodology

In this section we describe the proposed control chart. Section 3.1 details the specific profile monitoring problem we consider under a change-point framework. Section 3.2 details the construction of the proposed control chart, and section 3.3 describes the procedure for obtaining a control limit based solely on a set of known, IC profiles.

3.1 Change-point framework

Our underlying model,

$$y_i^t = \begin{cases} f(\mathbf{x}_i^t) + \epsilon_i^t & \text{for } t \leq \tau \\ h(\mathbf{x}_i^t) + \epsilon_i^t & \text{for } t > \tau, \end{cases} \quad (2)$$

of profile $\{(\mathbf{x}_i^t, y_i^t) : i \in [n]\}$ at time t is a special case of the model in (1), where $f : \mathbb{R}^d \rightarrow \mathbb{R}$ and $h : \mathbb{R}^d \rightarrow \mathbb{R}$ are respectively the IC and OOC functional relationships between the response y and the vector of explanatory variables \mathbf{x} , and τ is the unknown time of change-point. In this paper, we consider h of the form $h = \nu f + (1 - \nu)g$ for $\nu \in \mathbb{R}$ where the unknown g is called the OOC forcing function. Please recall from (1) that the errors ϵ^t in equations (1)-(2) are identically distributed with $\mathbb{E}[\epsilon^t] = \mathbf{0}$, $\text{Var}[\epsilon^t] = \sigma^2 \mathbf{I}_n$ and same correlation $\phi = \text{Corr}(\epsilon_i^r, \epsilon_i^s)$ for $r \neq s$. Again, \mathbf{I}_n denotes the $(n \times n)$ identity matrix. From either historical data or expert knowledge, we have $\{(\mathbf{X}^t, \mathbf{y}^t) : t = 1 - m, \dots, 0\}$ that are known to be m noise perturbed IC profiles. The goal is to correctly determine whether a process at time $T > 0$ is OOC using T new observed profiles $\{(\mathbf{X}^t, \mathbf{y}^t) : t = 1, \dots, T\}$ as well as m known IC profiles from historical data. That is, we wish to test the following hypothesis:

$$H_0 : \tau \geq T \text{ versus } H_a : \tau < T, \quad (3)$$

where H_0 is equivalent to $f = f^1 = \dots = f^T$ in (1). An ideal control chart method should be able to detect a profile being OOC whenever T is close to, but greater than, τ .

3.2 Constructing the eigenvector perturbation control chart

Consider the responses from w observed profiles $\{\mathbf{y}^t\}_{t=t_0+1}^{w+t_0}$ for some t_0 , and define $\mathbf{R} \in \mathbb{R}^{w \times w}$ to be the sample correlation matrix of these responses with leading eigenvector \mathbf{v} .

We can consider $\mathbf{\Gamma}$ to be the unperturbed matrix with leading eigenvector $\tilde{\mathbf{v}}$ with our perturbation matrix \mathbf{E} such that $\mathbf{R} = \mathbf{\Gamma} + \mathbf{E}$. If all w profiles are IC, then $\mathbf{\Gamma} = \mathbf{I}_w + (\gamma - 1)\mathbf{J}_w$, where \mathbf{J}_w is a $(w \times w)$ unit matrix, and $\gamma = \text{Corr}[y_i^r, y_i^s] = (\text{Cov}[f(\mathbf{x}_i^r), f(\mathbf{x}_i^s)] + \phi\sigma^2) / (\text{Var}[f(\mathbf{x}_i^r)] + \sigma^2)$ for $r \neq s$, where the Cov of the right hand side is taken with respect

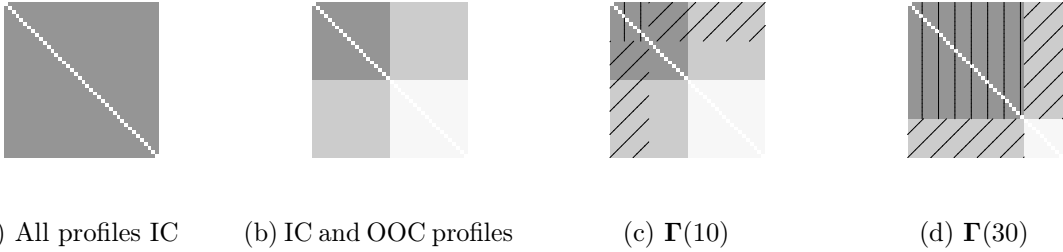


Figure 1: A visualization of $\mathbf{\Gamma}$, $\mathbf{\Gamma}(k_1)$ and $\mathbf{R}(k_1)$. The matrix $\mathbf{\Gamma}$ is shown in two scenarios in (a)-(b). In (b)-(d), $w = 40$, $\tau = 20$, $T = 40$. Vertically lined regions reflect the entries substituted from the correlation matrix obtained from the historical IC profiles. To compute $\mathbf{R}(k_1)$, the entries corresponding to the diagonally lined regions need to be computed due to substituting k_1 of the oldest observed profiles with historical IC profiles. For example, the columns of $\mathbf{\Gamma}(10)$ from left to right correspond to 10 historical profiles, 10 nonhistorical IC profiles, and 20 OOC profiles. The correlations of the last 30 profiles with the first 10 profiles under consideration are not in \mathbf{R} and need to be computed for $\mathbf{R}(10)$.

to the joint distribution of $(\mathbf{x}_i^r, \mathbf{x}_i^s)$. This ‘‘compound symmetry’’ form of $\mathbf{\Gamma}$ implies that its leading eigenvector is $\tilde{\mathbf{v}} = \frac{1}{\sqrt{w}}\mathbf{1}$. However, when \mathbf{R} is obtained from k_1^* IC profiles and $k_2^* = w - k_1^*$ OOC profiles, then $\mathbf{\Gamma}$ exhibits a block diagonal structure as shown pictorially in Figure 1b because $\Gamma_{r,s}$ is

$$\Gamma_{r,s} = \text{Corr}[y_i^u, y_i^v] = \frac{\text{Cov}[f(\mathbf{x}_i^u), h(\mathbf{x}_i^v)] + \phi\sigma^2}{\sqrt{(\text{Var}[f(\mathbf{x}_i^u)] + \sigma^2)(\text{Var}[h(\mathbf{x}_i^v)] + \sigma^2)}}, \text{ if } r \leq k_1^* < s \quad (4)$$

as (\mathbf{x}_i^u, y_i^u) at u is IC and (\mathbf{x}_i^v, y_i^v) at v is OOC. Similarly, if $r, s \leq k_1^*$, that is, both are IC profiles with $u, v \leq \tau$, then $\text{Corr}[y_i^u, y_i^v] = (\text{Cov}[f(\mathbf{x}_i^u), f(\mathbf{x}_i^v)] + \phi\sigma^2) / (\text{Var}[f(\mathbf{x}_i^u)] + \sigma^2)$ and $\text{Corr}[y_i^u, y_i^v] = (\text{Cov}[h(\mathbf{x}_i^u), h(\mathbf{x}_i^v)] + \phi\sigma^2) / (\text{Var}[h(\mathbf{x}_i^u)] + \sigma^2)$ if both are OOC profiles with $u, v > \tau$. As the row sums of $\mathbf{\Gamma}$ for the first k_1^* rows are the same (the same is true for the last k_2^* rows), $\tilde{\mathbf{v}} \propto \xi^*\mathbf{u}_1^* + \mathbf{u}_2^*$ where ξ^* is a constant, $\mathbf{u}_1^* = \sum_{l=1}^{k_1^*} \mathbf{e}_l$, $\mathbf{u}_2^* = \sum_{l=k_1^*+1}^w \mathbf{e}_l$, and \mathbf{e}_l is the l th standard basis vector.

Now we leverage the differences between the leading eigenvectors under the IC scenario and under the scenario with a mix of IC and OOC profiles to create our monitoring statistic. Unlike under the IC condition when $\|\mathbf{v} - \frac{1}{\sqrt{w}}\mathbf{1}\|_2$ should be small, \mathbf{v} should be very different from $\frac{1}{\sqrt{w}}\mathbf{1}$ when w profiles include at least one OOC profile because in this setting \mathbf{v} is close to $(\xi^*\mathbf{u}_1^* + \mathbf{u}_2^*) / \|\xi^*\mathbf{u}_1^* + \mathbf{u}_2^*\|_2$. As such, in this setting, we expect our chosen monitoring statistic $\|\mathbf{v} - \frac{1}{\sqrt{w}}\mathbf{1}\|_2$ to be large. Practical considerations include: (1) an $O(wn)$ time update scheme for \mathbf{R} between timesteps (as opposed to a naïve $O(w^2n)$ execution); (2) specifying how to compute the leading eigenvector of \mathbf{R} ; (3) accounting for the possible failure of the control chart to correctly flag a profile as being OOC by time $T > \tau$. As \mathbf{R} is computed on a moving window, the update scheme merely computes one new row/column’s worth of entries and ejects the row/column corresponding to the oldest profile in the window. The second consideration is addressed in the supplementary materials.

Regarding the third issue, with the current procedure, all w profiles considered would be OOC at time $\tau + w$, and the control chart no longer would be able to detect an OOC profile as this scenario looks identical to the one where all w profiles are IC. To mitigate this issue, we can sample without replacement k_1 of the m historical, IC profiles to replace the $k_1 > 0$ oldest profiles of the w profiles being considered. Doing so guarantees an IC reference frame with which to compare an OOC profile. Assuming \mathbf{R} has already been computed for a set of w profiles at time T , replacing k_1 of the oldest observed profiles modifies the sample correlation matrix. Denote $\mathbf{R}(k_1)$ be such a correlation matrix derived from \mathbf{R} through this replacement procedure, $\mathbf{\Gamma}(k_1)$ be the corresponding population correlation matrix, and let $\mathbf{v}(k_1)$ and $\tilde{\mathbf{v}}(k_1)$ be the leading eigenvectors of $\mathbf{R}(k_1)$ and $\mathbf{\Gamma}(k_1)$, respectively. Figure 1 provides a visualization for two such instances of $\mathbf{\Gamma}(k_1)$. As the notation suggests, $\tilde{\mathbf{v}}(k_1)$ is dependent on k_1 . Specifically, $\tilde{\mathbf{v}}(k_1) \propto \xi(k_1)\mathbf{u}_1 + \mathbf{u}_2$ where \mathbf{u}_1 and \mathbf{u}_2 are defined similarly to \mathbf{u}_1^* and \mathbf{u}_2^* . The technical details for this derivation are in the supplementary materials. As $\tilde{\mathbf{v}}(k_1)$ is a function of k_1 , the distribution of $\mathbf{v}(k_1)$ is also a function of k_1 , and hence, the distribution of $\|\mathbf{v}(k_1) - \frac{1}{\sqrt{w}}\mathbf{1}\|_2$ is also a function of k_1 . So a choice of k_1 is required, but as shown in the supplementary materials, the distribution of $\|\mathbf{v}(k_1) - \frac{1}{\sqrt{w}}\mathbf{1}\|_2$ is also a function of the two values of $\text{Corr}[y_i^u, y_i^v]$ where $v > \tau$, which cannot be known before monitoring begins. Therefore, k_1 cannot be chosen to maximize the difference between $\frac{1}{\sqrt{w}}\mathbf{1}$ and a normalized $\xi(k_1)\mathbf{u}_1 + \mathbf{u}_2$. We choose instead to select L , evenly spaced values of k_1 (say $K = \{1, \lfloor \frac{w}{L} \rfloor, 2 \lfloor \frac{w}{L} \rfloor, \dots, (L-2) \lfloor \frac{w}{L} \rfloor, w-1\}$), and use $\max_{k_1 \in K} \|\mathbf{v}(k_1) - \frac{1}{\sqrt{w}}\mathbf{1}\|_2$ as the monitoring statistic. We combine all of the aforementioned modifications to the original monitoring scheme as detailed in the Algorithm 1.

3.3 Determining control limits

The proposed control chart needs an upper control limit U wherein if the monitoring statistic exceeds U , we claim at least one of the w observed profiles to be OOC. A nonasymptotic bound on EP found in the literature could be a candidate control limit. Assuming we knew the quantities used in these bounds (e.g., $\|\mathbf{E}\|$) under IC conditions, the monitoring statistic would be guaranteed never to exceed the bound under IC conditions. Using bounds found in the literature as control limits poses a problem: their hidden constants need to be found in order to obtain a control limit. These hidden constants are often too large making detecting of an OOC profile difficult. Another method is required to determine control limits, and we use the existence of these bounds to motivate our choice of control limit.

Assume a large sample of EPs p_1, \dots, p_N under the IC condition are available to inform our control limit. Based on theory from Morales-Jimenez et al. (2021) and empirical observations, we can reasonably assume IC EPs to lie in an interval $(0, C] \subset (0, 2)$ with C small. Ideally, we want U large enough to result in a low probability of false alarm (PFA), but not so large as to be unable to detect an OOC profile. We want to choose $U \leq C + c$ for some small $c > 0$. If $U < C$, then PFA will be positive and hopefully small. If $U > C$, then $ARL_0 = \infty$, and we would want to avoid a loss of sensitivity by choosing U to be close to C as possible. We adopt an empirically useful approximation of the distribution of EPs under the IC condition to achieve this second desired effect. Specifically, we set $U = F^{-1}(q)$ for an aggressively large choice of q where F is the CDF of a normal distribution fitted to the

Algorithm 1: Eigenvector Perturbation Control Chart

Given: – Historical data: $\mathbf{X}^t, \mathbf{y}^t$ where $\mathbf{y}^t \in \mathbb{R}^n$, $\mathbf{X}^t \in \mathbb{R}^{n \times p}$, $t \in \{1 - m, \dots, 0\}$
– Upper control limit: $U > 0$
– A nonempty $K \subset [w - 1]$
– Tolerance for power iteration detector: ζ
– Window size: $w \leq m$

Do:
Compute the sample correlation matrix $\mathbf{R}^* \in \mathbb{R}^{m \times m}$ of the historical profiles.
Set \mathbf{R} to be the last w columns and rows of \mathbf{R}^*
 $S = -1$; $T = 1$
#Conduct process monitoring
while $S < U$
 Observe $\mathbf{y}^T \in \mathbb{R}^n$; update \mathbf{R} to reflect correlations of $\{\mathbf{y}^{T-w+1}, \dots, \mathbf{y}^T\}$
 for every k_1 in K
 if $T < w - k_1$, set $\mathcal{I} = [m - w + k_1 + T]$ **else** set $\mathcal{I} = [m]$
 Sample k_1 indices j_1, \dots, j_{k_1} from \mathcal{I} without replacement; set $\mathbf{R}(k_1) = \mathbf{R}$
 Replace the first k_1 rows/columns of $\mathbf{R}(k_1)$ with the j_1, \dots, j_{k_1} rows/columns of \mathbf{R}^*
 $\mathbf{v}(k_1) = \text{modified_power_iteration_detector}\left(\mathbf{R}(k_1), \frac{1}{\sqrt{w}}\mathbf{1}, \zeta\right)$
 $S = \max_{k_1 \in K} \|\mathbf{v}(k_1) - \frac{1}{\sqrt{w}}\mathbf{1}\|_2$
 if $S > U$, claim change point occurred **else** set $T = T + 1$

p_1, \dots, p_N using typical moment estimates. The aggressive choice of q will result in a large U , and the light tail of a Gaussian will limit how large $U - C$ can become should the choice of c result in $U > C$. As the maximum of a set of EPs also shares similar boundedness properties as the N EPs, we apply this “quantile trick” to a large set of IC monitoring statistics S_1, \dots, S_N . Bootstrapping can be used to obtain the required large sample of monitoring statistics, with one such approach detailed in the supplementary materials.

4 Simulations

In this section, we detail results from simulation studies. The first simulation study compares the EP control chart against existing nonparametric and semiparametric profile monitoring methods. The second simulation study aims to identify conditions that degrade performance of our method. Supplementary materials address technical details regarding control limit calibration, scenario details, two competitors’ performances, an illustrative example using distinct, dependent predictors between time steps, and effect size calibration.

4.1 The general setup for the simulation studies

Each simulation study consists of a set of scenarios that typically cover all possible combinations of factors of interest. For each scenario (simulation model), we simulate 100 replications (trials) of the sequence of profiles from the underlying simulation model and the corresponding process monitoring to obtain the Monte Carlo estimates of the *ARL* and *FAR* of each method. For each replication/trial, m historical profiles were randomly generated, and a control limit was set. How the control limit was determined was dependent on the monitoring scheme used. Once a control limit was established, we began monitoring, and a new profile was generated for each time step. If a false alarm occurred, the control

chart was restarted as if monitoring had just begun. The time of the last IC profile τ was fixed remaining unaffected by the number of false alarms. Monitoring ended either when the control chart raised an alarm after time τ or if it failed to provide a true alarm after time T_{timeout} . If t_i^* denotes the time when a true alarm occurs for the i th trial, the Monte Carlo estimate of ARL_1 is $\frac{1}{100} \sum_{i=1}^{100} (t_i^* - \tau)$, assuming that all 100 trials terminated prior to T_{timeout} . The estimate of the FAR is the proportion of alarms that are false alarms.

We need to consider the effects various types of functions (f, h) have on the performance of profile monitoring methods in order to compare them. We use a signal-to-noise ratio (SNR) as our primary choice of effect size, though other related effect sizes are considered. We define the SNR as $\text{Var}[f(\mathbf{x}) - h(\mathbf{x})]/\sigma^2$, and the variance is taken with respect to a random \mathbf{x} . For the remainder of the paper, we refer to $\text{Var}[f(\mathbf{x}) - h(\mathbf{x})]$ as $\text{Var}[f - h]$ for brevity. Similarly, we refer to $\text{Cov}[f(\mathbf{x}), h(\mathbf{x})]$ as $\text{Cov}[f, h]$. Unless otherwise stated, we use $\epsilon^t \sim N(\mathbf{0}, \mathbf{I})$ for all t , so the SNR is simply $\text{Var}[f - h]$. Also unless otherwise stated, we assume the OOC functional relationship h to be an affine combination of f and some OOC forcing function g , where the affine combination parameter is chosen to achieve the desired effect sizes such as SNR and between-profile correlation.

4.2 Comparing with other approaches

We compare the proposed EP control chart with competing nonparametric control charts in this section and demonstrate its superior performance. The competing control charts are the SIM based approach from Iguchi et al. (2021), the SVR method of Li et al. (2019), a wavelet based method of Chicken et al. (2009), and a PCA based control chart from Colosimo and Pacella (2010) hereinafter referred to as the PCA control chart. We also implemented the methods of Zou et al. (2008) and Qiu et al. (2010), but we place their results in the supplementary materials due to computational issues they faced preventing monitoring from occurring. We only use the simulation models where error distributions are independent over time with $\text{Corr}[\epsilon_i^r, \epsilon_i^s] = 0$, and common $\mathbf{x}_i^t = \mathbf{x}_i$ for all time-points t are sampled independently for $i = 1, \dots, n$ from a common p -dimensional multivariate distribution. So, the expression of $\Gamma_{r,s}$ in (4) is only $\text{Cov}[f(\mathbf{x}), h(\mathbf{x})]/\sqrt{\text{Var}[f(\mathbf{x})]\text{Var}[h(\mathbf{x})]}$ if one is from IC and another from OOC profiles. Even though our method is equipped for process monitoring under a very general set-up, especially when \mathbf{x}_i^t are different over time and $\text{Corr}[\epsilon_i^r, \epsilon_i^s] = \phi \neq 0$ for $r \neq s$, we use this simpler simulation model because we would like to make a fair comparison with competing methods which were not meant to accommodate these general modeling assumptions of our method.

4.2.1 Multivariate predictors

We begin with comparing nonparametric profile monitoring methods with multiple predictors. The profile monitoring methods were used on each scenario of a full-factorial design of factors and levels taken from Iguchi et al. (2021). We summarize the results in Table 1 by listing the range of FAR and ARL_1 across all scenarios of the experiment with noninteger values being rounded.

The PCA control chart results are not listed as it failed to raise a true alarm by

Table 1: Performance of non/semi-parametric profile monitoring with multiple predictors.

Method	ARL_0	τ	Range of observed FAR	Range of observed ARL_1	Fast Calibration?
Li et al. (2019)	200	30	(0.17, 0.37)	(4.24, 4.86)	No
	370	30	(0.07, 0.34)	(4.37, 5.39)	No
Iguchi et al. (2021)	200	30	(0.07, 0.25)	(1, 2.44)	No
	370	30	(0.01, 0.11)	(1, 2.75)	No
Eigenvector	200	30	(0.17, 0.69)	(1, 1)	No
Perturbation	370	30	(0.01, 0.55)	(1, 1)	No
	$> 5 \times 10^6$	30	(0, 0)	(1, 1)	Yes
	$> 5 \times 10^6$	10^4	(0, 0.01)	(1, 1)	Yes

$T_{\text{timeout}} = 11500$ in 3195 of the 3200 trials conducted across 32 scenarios. Observe the proposed method using a control limit obtained from bootstrapping outperformed its competitors: the sensitivity of the proposed method is not affected by dramatically increasing the ARL_0 . Lower bounds for the ARL_0 of the EP control chart using the control limit obtained through bootstrapping are listed in the supplementary materials. The competing methods either cannot calibrate to such a large ARL_0 or underperform with respect to FAR and ARL_1 . If the SIM and SVR methods could be calibrated to an $ARL_0 > 5 \times 10^6$, the FAR could certainly be competitive with the EP control chart. Doing so, however, comes at the cost of increasing ARL_1 as demonstrated by increasing the ARL_0 from 200 to 370. Even at $ARL_0 = 370$, both of these competing methods could not achieve an $ARL_1 = 1$ across all scenarios in the computer experiment, while the EP control chart achieved this feat. As a low FAR should be expected from setting $\tau = 30$ when a control chart is calibrated to $ARL_0 > 5 \times 10^6$, we increased τ to 10^4 for the proposed method. Even at a large value of τ , the FAR is extremely small. In fact, 13 of 16 scenarios resulted in no false alarms.

4.2.2 Univariate predictors

As there are competing methods designed with one predictor in mind, we compare them against the proposed method with a single predictor. The smallest lower bound on the observed ARL_0 for the EP control chart in Section 4.2.1 was 5010603 so the PCA control chart was calibrated to such an ARL_0 in addition to ARL_0 of 200 and 370. We set T_{timeout} to be 10500, 11500, and 3000 for the EP, PCA, and wavelet control charts, respectively.

	$ARL_0 \backslash \tau$	PCA			Wavelet		EP ($w \in \{20, 40\}$)		
		0	30	10^4	0	30	0	30	10^4
Range of observed FAR	200	-	(0, 0)	(0, 0)	-	(0.04, 0.15)	-	*	*
	370	-	(0, 0)	(0, 0)	-	(0.04, 0.15)	-	*	*
	"large"	-	(0, 0)	(0, 0)	-	*	-	(0, 0)	(0, 0.07)
Max observed ARL_1	200	∞	∞	∞	3.34	447.27	-	*	*
	370	∞	∞	∞	3.37	455.20	-	*	*
	"large"	∞	∞	∞	-	*	12.70	12.97	12.86
Scenarios with $ARL_1 = 1$	200	12/16	12/16	12/16	13/16	13/16	-	*	*
	370	13/16	13/16	13/16	13/16	13/16	-	*	*
	"large"	10/16	10/16	10/16	-	*	20/32	20/32	20/32

Table 2: A comparison of nonparametric profile monitoring methods with a single predictor

We summarize the results in Table 2. Although the PCA control chart was optimal in ARL_1 in some scenarios, it often was unable to raise a true alarm. The wavelet control

chart detected an out-of-control profile in all scenarios, but as τ increased, the ARL_1 greatly increased (e.g., from 3.37 to 446) in six scenarios. The wavelet control chart leveraging all previously observed profiles explains the $O(T^2)$ computational complexity at time T (and the reason for omitting calibrating to $ARL_0 = 5010603$) and may also explain the dependence of its ARL_1 on τ . The EP control chart using the “quantile trick” should result in an extremely large ARL_0 per the simulation study in Section 4.2 and yields respectable FAR and ARL_1 . We claim the EP control chart is preferable to the two alternatives as multiple predictors are allowed, long run lengths are feasible, and achieves good performance.

4.3 Investigating the boundaries of “good” performance

Given the promising results thus far, we now investigate settings which are difficult for the EP control chart. In Section 4.3.1, we find combinations of control chart parameters and properties of the IC and OOC profiles which are difficult for the EP control chart. The EP control chart loses its good performance under conditions which are the result of windowing, a consequence of monitoring correlations, or truly difficult for any nonparametric profile monitoring procedure. We show via simulation robustness to moderate levels of within profile correlated errors, small SNRs, and heavy tailed errors in Section 4.3.2.

4.3.1 Parameters of the control chart and the profiles

In the previous subsection, we demonstrated the superior performance of the EP control chart. In this subsection we explore the scenarios where the performance of the EP control chart degrades and no longer achieves a zero FAR and ARL_1 of one.

There are some scenarios in which we should expect the EP control chart to fail to detect an OOC profile such as $h \propto f$ or $h = f + c$ for some constant c . We consider the first such difficult scenario. As such, we consider the correlation $\rho[f, h]$ between the IC and OOC functional relationships, f and h , respectively. Additionally, the variance of the sample correlation of $\mathbf{y}^r, \mathbf{y}^s$, with $r, s \leq \tau$ depends on $\text{Var}[f]/\sigma^2$, so $\text{Var}[f]$ is also included.

In this subsection we consider profiles where the functional relationship in a profile are zero intercept quadratic polynomials. That is, we assume f, g , and h are of the following form: $\mathbf{x}^\top \mathbf{A} \mathbf{x} + \mathbf{a}^\top \mathbf{x}$ where $\mathbf{A} \in \mathbb{R}^{d \times d}$, $\mathbf{a} \in \mathbb{R}^d$. The factors and levels of the simulation study are outlined in the supplementary materials. For the simulation study, \mathbf{X} was randomly chosen from $\text{Unif}([0, 1]^{25})$ at the beginning of each trial and held fixed for all time steps t . Scenarios consisted of all possible combinations of $\tau \in \{0, 30, 10^4\}$, $\log_2(n) \in \{7, 8, 9\}$, $m \in \{20, 40\}$, $m/w \in \{1, 2\}$, $\text{SNR} \in \{3, 5\}$, $\text{Var}[f] \in \{2, 4, 6\}$, $\rho(f, h) \in \{0.75, 0.9\}$, and the convexity of h with respect to f and g (i.e., if $\nu \in [0, 1]$). Figure 2 shows the estimates of the FAR across the relevant factors in the experimental design which affect IC performance. As expected, the FAR for $\tau = 30$ was zero in all but one case. When $\tau = 10^4$, we observe excellent performance when $n = 512$. Also notice as m/w increased, the FAR decreased. Finally, as $\text{Var}[f]$ increased with n fixed, the FAR tended to decrease. Therefore, a practitioner can decrease the FAR by increasing n , m , m/w , and, if possible, $\text{Var}[f]/\sigma^2$.

Figure 2 depicts the approximations of the ARL_1 across the relevant factors in the experiment which influence OOC performance. As expected, ARL_1 decreased with increasing

n , m/w , or $\rho(f, h)$. The ARL_1 did not decrease uniformly with increasing SNR and $\text{Var}[f]$, and this counterintuitive behavior is a result of some nonintuitive relationships between SNR, $\text{Var}[f]$, and $\rho[f, h]$ which is explained in the supplementary materials.

We should expect poor performance when n is small, $\rho[f, h] \approx 1$, and $\nu > 1$. For example, when $n = 64$ $\rho[f, h] = 0.9$, $\text{Var}[f] < 6$, and $\nu > 1$, 30 trials of 4800 trials across the relevant 48 treatment combinations in the experimental design failed to raise an alarm by time $t = 10500$. Additionally, we repeated the same simulation experiment but used smaller and negative correlations (with $\rho[f, h] \in \{-1, -0.75, \pm 0.5, \pm 0.3, 0\}$). For all of these additional settings of $\rho[f, h]$, the control chart demonstrated optimal performance with $ARL_1 = 1$.

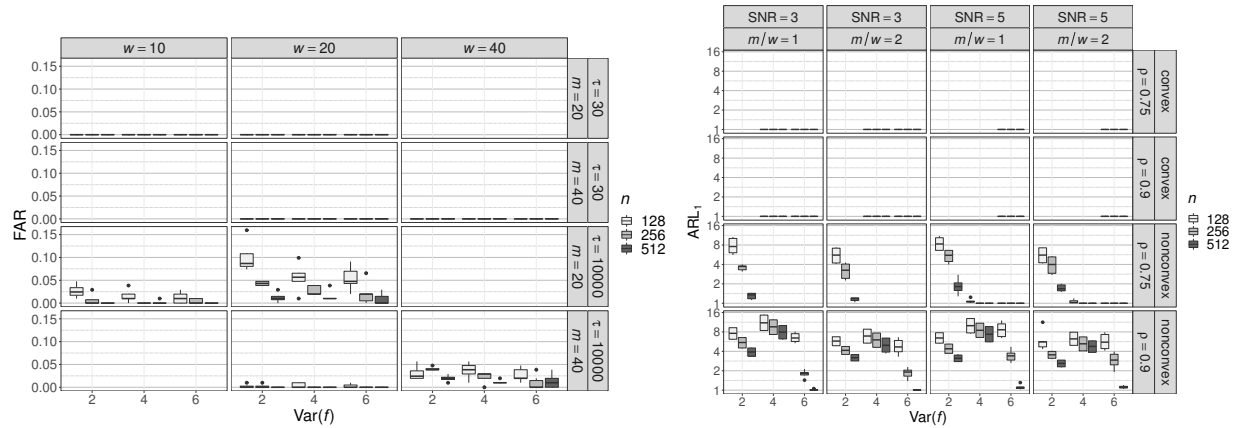


Figure 2: Boxplots of the FARs (left) and ARL_1 (right) for the proposed control chart for the simulation study in Section 4.2.1. Each boxplot on the left is drawn using the FARs across the various choices of SNR, $\rho[f, h]$, and choice of a convex combination of f and h , as these quantities affect alarms after τ and do not affect the FAR. Each boxplot on the right is drawn using the ARL_1 across the various choices of τ and m . These factors are omitted in the facet plot as τ and m have little to no effect on ARL_1 . Flat boxplots with no outliers indicate instances of zero false alarms (left) or $ARL_1 = 1$ (right) across all relevant treatment combinations. Scenarios not in the experimental design result in empty plots.

4.3.2 Other difficult scenarios

In this subsection, we consider three other difficult scenarios and present the results of these simulations in Figure 3. The first scenario uses heavy tailed errors (i.e., t-distributed with varying degrees of freedom). The performance of the EP control chart is unsatisfactory when the errors have less than five moments, but begins to achieve good performance when the errors have more than four moments. This transition in performance agrees with the theory in EP for covariance and correlation matrices which typically assumes the data have greater than four moments. The second scenario involves within-profile correlation. We place an AR(1) structure on the errors given their order of appearance within a profile (i.e., $\text{Corr}[\epsilon_i, \epsilon_j] = \psi^{|i-j|}$). We see the EP control chart can handle moderate levels of within-profile correlation as measured by the autocorrelation parameter. The third scenario

considers a case where the SNR is small but $\text{Var}[f]$ is large. The EP control chart only performs poorly once the SNR reaches a value of 0.2, which is exceptionally small.

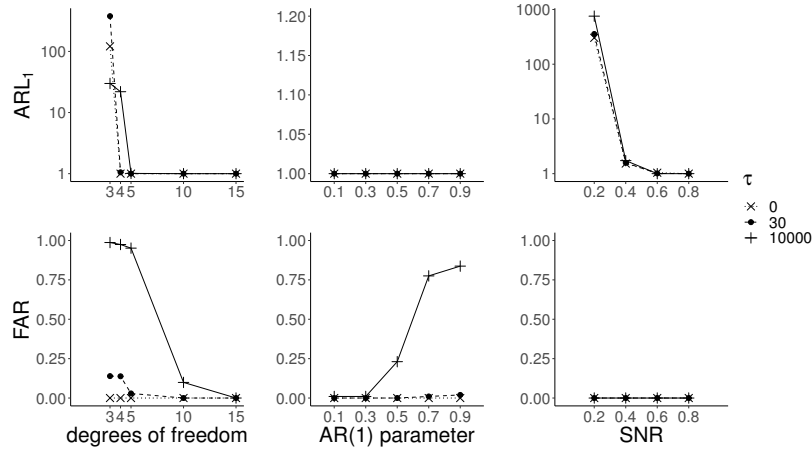


Figure 3: EP control chart performance in difficult scenarios. (left) Errors are t-distributed. (middle) Within profile correlation with AR(1) errors. (right) $\text{SNR} < 1$ with $\text{Var}[f] = 6$.

5 Real World Dataset Application

We apply the EP and PCA control charts on a robot arm approaching and grasping an object before transferring it to a new location and ungrasping it (Dua and Graff 2017; Camarinha-Matos et al. 1996). Force and torque measurements are collected along three axes every 315 ms for 4.725s under successful and failed attempts. The supplementary materials contain visualizations and details on the dataset and its IC and OOC scenarios.

The robotic dataset is well suited for demonstrating our EP control chart due to its unique combination of small sample sizes and large variance ratio, $\text{Var}[f]/\sigma^2$. Using timestamps and measurement types as predictors, which do not change between attempts, an executed task results in a profile with $n = 90$. With only 18 of the 21 normally executed tasks being considered to form IC profiles after data cleaning, m , n , and w are relatively small implying poor EP control chart performance unless $\text{Var}[f]/\sigma^2$ is exceptionally large. The observed variance ratio under normal operating conditions meets this condition with $\widehat{\text{Var}}[\hat{f}]/\hat{\sigma}^2 = 72.8$. Having such a large variance ratio is intuitive for robotic arm tasks: the variability between repeated attempts is minimal due to the precision of robotic movements, resulting in a small σ^2 . At the same time, tasks requiring substantial movement produce large variability in sensor measurements, leading to large $\text{Var}[f]$. As such, the robot arm dataset provides an ideal context where the EP control chart can excel despite small m , n , and w .

For simulations, we used $(w, m) \in \{4, 5, 6\} \times \{11, 12, 13\}$, $\tau = 18 - m$, and three different types of collision with the robot arm to form OOC scenarios. For each trial, we randomly permute the IC profiles, assign the first m to be historical IC profiles, and let the rest be observed in an online fashion. The OOC profiles are sampled without replacement.

Using the PCA control chart no false alarms were raised, but we often observed $ARL_1 > 1$. The ARL_1 averaged over all of the scenarios were 1.46, 1.53, and 2.12 for ARL_0 of 200, 370, and 5010603, respectively. Using the EP control chart, $ARL_1 = 1$ was observed for all scenarios. Only four of the 27 scenarios simulated resulted in positive FARs, all less than 0.02, occurring when $(w, m) \in \{(4, 11), (4, 12), (5, 11), (6, 11)\}$. As seen in Section 4.2.1, we suspect the small w and m contribute to the positive FAR despite the small τ .

6 Discussion

We established a new nonparametric profile monitoring tool using EP to deal with a vector of quality characteristics that are a scalar function of multiple explanatory variables. For existing nonparametric profile monitoring methods for this situation, a Monte Carlo approach is commonly required to calibrate control limits. For such approaches, calibrating to large ARL_0 on the order of 10^6 is infeasible and impractical. Unlike the profile monitoring in the literature that typically calibrates control limits to ARL_0 of 200 or 370, our proposed profile monitoring method can quickly calibrate to a very large $ARL_0 > 10^6$. Usually, the ARL_1 increases as the ARL_0 increases. Despite achieving such a large ARL_0 , our EP based control chart suffers little loss in ARL_1 . The success of the EP control chart lies in the sensitivity of $\|\mathbf{v} - \frac{1}{\sqrt{w}}\mathbf{1}\|$ to changes from a one-block structure of \mathbf{R} and the ability to obtain large specificity (by decreasing variability of the entries of \mathbf{R}) with sufficiently large n or $\text{Var}[f]/\sigma^2$. Large values of m and m/w help in decreasing the FAR and increasing the efficiency of the bootstrapping used to find control limits. Performance degrades under truly difficult situations such as when n , m , $\text{Var}[f]/\sigma^2$, or $|\text{Corr}[f(\mathbf{x}_i^r), f(\mathbf{x}_i^s)] - \text{Corr}[f(\mathbf{x}_i^r), h(\mathbf{x}_i^t)]|$ for $r, s \leq \tau < t$ are small. The robot failures application shows increasing one of these quantities can compensate for a small value of one of the other quantities.

Future work may include monitoring not just correlations but also if $\nu = 1$. The regime of (n, m) for our method contrasts with methods requiring m to be large (≥ 500) and allowing n to be small (e.g., Qiu et al. (2010)). Achieving similar performance for small n remains an open problem. It is not uncommon for time series data to be autocorrelated as opposed to the equicorrelated structure explored in this paper, so the proposed EP control chart could be modified to handle a different correlation structure. Relaxing the need for dependent predictors $\mathbf{x}^r, \mathbf{x}^s, r \neq s$ would also be valuable.

Competing Interests

The authors report there are no competing interests to declare.

SUPPLEMENTARY MATERIAL

Supplementary manuscript: Contains miscellaneous mathematical details, pseudocode for the proposed procedures, the experimental designs used in the simulation studies, and miscellaneous simulation results.

Code for the simulation study using quadratic profiles R code to execute the EP control chart in the simulation study in Section 4.3.2.

References

- Amiri, A., W. A. Jensen, and R. B. Kazemzadeh (2009, Oct). A case study on monitoring polynomial profiles in the automotive industry. *Quality and Reliability Engineering International* 26(5), 509–520.
- Bersimis, S. and A. Sachlas (2022). Surveilling public health through statistical process monitoring: A literature review and a unified framework. *Communications in Statistics: Case Studies, Data Analysis and Applications* 8(3), 515–543.
- Camarinha-Matos, L., L. Lopes, and J. Barata (1996). Integration and learning in supervision of flexible assembly systems. *IEEE Transactions on Robotics and Automation* 12(2), 202–219.
- Chen, Y., Y. Chi, J. Fan, C. Ma, et al. (2021). Spectral methods for data science: A statistical perspective. *Foundations and Trends® in Machine Learning* 14(5), 566–806.
- Chicken, E., J. J. Pignatiello, and J. R. Simpson (2009). Statistical process monitoring of nonlinear profiles using wavelets. *Journal of Quality Technology* 41(2), 198–212.
- Colosimo, B. M. and M. Pacella (2007). On the use of principal component analysis to identify systematic patterns in roundness profiles. *Quality and Reliability Engineering International* 23(6), 707–725.
- Colosimo, B. M. and M. Pacella (2010). A comparison study of control charts for statistical monitoring of functional data. *International Journal of Production Research* 48(6), 1575–1601.
- Colosimo, B. M., Q. Semeraro, and M. Pacella (2008, Jan). Statistical process control for geometric specifications: on the monitoring of roundness profiles. *Journal of Quality Technology* 40(1), 1–18.
- Davis, C. and W. M. Kahan (1970). The rotation of eigenvectors by a perturbation. III*. 7(1).
- Dua, D. and C. Graff (2017). UCI machine learning repository.
- Hackl, P. and J. Ledolter (1991). A control chart based on ranks. *Journal of Quality Technology* 23(2), 117–124.
- Hung, Y. C., W. C. Tsai, S. F. Yang, S. C. Chuang, and Y. K. Tseng (2012). Nonparametric profile monitoring in multi-dimensional data spaces. *Journal of Process Control* 22(2), 397–403.

- Iguchi, T., A. F. Barrientos, E. Chicken, and D. Sinha (2021). Nonlinear profile monitoring with single index models. *Quality and Reliability Engineering International* 37(7), 3004–3017.
- Imhoff, M. and S. Kuhls (2006, May). Alarm algorithms in critical care monitoring. *Anesthesia & Analgesia* 102(5), 1525–1537.
- Jin, J. and J. Shi (1999, Nov). Feature-preserving data compression of stamping tonnage information using wavelets. *Technometrics* 41(4), 327–339.
- Kang, L. and S. L. Albin (2000, Oct). On-line monitoring when the process yields a linear profile. *Journal of Quality Technology* 32(4), 418–426.
- Kuchibhotla, A. and R. Patra (2020). Efficient estimation in single index models through smoothing splines. *Bernoulli* 26(2), 1587–1618.
- Li, C. I., J. N. Pan, and C. H. Liao (2019). Monitoring nonlinear profile data using support vector regression method. *Quality and Reliability Engineering International* 35(1), 127–135.
- Maleki, M. R., A. Amiri, and P. Castagliola (2018, Dec). An overview on recent profile monitoring papers (2008–2018) based on conceptual classification scheme. *Computers & Industrial Engineering* 126, 705–728.
- McGinnity, K., E. Chicken, and J. J. Pignatiello (2015). Nonparametric changepoint estimation for sequential nonlinear profile monitoring. *Quality and Reliability Engineering International* 31(1), 57–73.
- Morales-Jimenez, D., I. M. Johnstone, M. R. McKay, and J. Yang (2021). Asymptotics of eigenstructure of sample correlation matrices for high-dimensional spiked models. *Statistica Sinica* 31(2), 571.
- Qiu, P., X. Zi, and C. Zou (2018). Nonparametric dynamic curve monitoring. *Technometrics* 60(3), 386–397.
- Qiu, P., C. Zou, and Z. Wang (2010). Nonparametric profile monitoring by mixed effects modeling. *Technometrics* 52(3), 265–277.
- Viveros-Aguilera, R., S. H. Steiner, and R. J. MacKay (2014). Monitoring product size and edging from bivariate profile data. *Journal of Quality Technology* 46(3), 199–215.
- Wang, Y., Y. Mei, and K. Paynabar (2018). Thresholded multivariate principal component analysis for phase I multichannel profile monitoring. *Technometrics* 60(3), 360–372.
- Williams, J. D., W. H. Woodall, and J. B. Birch (2007, Dec). Statistical monitoring of nonlinear product and process quality profiles. *Quality and Reliability Engineering International* 23(8), 925–941.

- Woodall, W. H. and F. W. Faltin (2019). Rethinking control chart design and evaluation. *Quality Engineering* 31(4), 596–605.
- Zou, C., F. Tsung, and Z. Wang (2008). Monitoring profiles based on nonparametric regression methods. *Technometrics* 50(4), 512–526.

Supplementary Material: Profile Monitoring via Eigenvector Perturbation

Takayuki Iguchi*

Department of Statistics, Florida State University
and

Andrés F. Barrientos

Department of Statistics, Florida State University
and

Eric Chicken

Department of Statistics, Florida State University
and

Debajyoti Sinha

Department of Statistics, Florida State University

November 6, 2024

Abstract

In Statistical Process Control, control charts are often used to detect undesirable behavior of sequentially observed quality characteristics. Designing a control chart with desirably low False Alarm Rate (FAR) and detection delay (ARL_1) is an important challenge especially when the sampling rate is high and the control chart has an In-Control Average Run Length, called ARL_0 , of 200 or more, as commonly found in practice. Unfortunately, arbitrary reduction of the FAR typically increases the ARL_1 . Motivated by eigenvector perturbation theory, we propose the Eigenvector Perturbation Control Chart for computationally fast nonparametric profile monitoring. Our simulation studies show that it outperforms the competition and achieves both $ARL_1 \approx 1$ and $ARL_0 > 10^6$.

Keywords: Statistical Process Control, Nonparametric Profile Monitoring, Change-point Detection, Alarm Fatigue, False Alarm Rate (FAR)

*T. Iguchi has changed affiliation to the Air Force Institute of Technology, but the work was performed while at Florida State University. This work was supported by the Office of the Secretary of Defense, Directorate of Operational Test and Evaluation under Grant FA8075-14-D-0019 and the Test Resource Management Center under the Science of Test research program under Grant FA807518F1525. The views expressed in this article are those of the author and do not reflect the official policy or position of the United States Air Force, Department of Defense, or the U. S. Government.

1 Overview

The supplementary materials are organized in the following fashion. Section 2 derives the eigenspace for the population correlation matrix under the scenario where all profiles are IC and under the scenario where there is a mix of IC and OOC profiles in the window. Section 3 discusses computational considerations for the proposed control chart. Section 4 details the algorithms involved with the control chart. Section 6 covers the details of the simulation study comparing methods with multiple predictors. Section 7 discusses details of a simulation study where quadratic profiles are used for IC and OOC profiles. Section 9 details the methodology for calibrating profiles to desired effect sizes. Section 10 covers a few details regarding the Robot Failures dataset and a note on cleaning the dataset.

2 Eigenspace of Γ

Assume there are k_1 in-control profiles and k_2 out-of-control profiles being considered in the sample correlation matrix. Let γ_1 be the population correlation of two in-control profiles (i.e., $\gamma_1 = (\text{Cov}[f(\mathbf{x}_i^r), f(\mathbf{x}_i^s)] + \phi\sigma^2) / (\text{Var}[f(\mathbf{x}_i^r)] + \sigma^2)$ for $r, s \leq \tau$). Similarly, let γ_2 be the population correlation where two out-of-control profiles are being considered and let $\gamma_{12} = \gamma_{21}$ be the population correlation of an in-control and out-of-control profile. As the population correlation matrix is going to have a block diagonal structure (aside from the diagonal), let us call $\mathbf{u}_1 = \sum_{i=1}^{k_1} \mathbf{e}_i$ and $\mathbf{u}_2 = \sum_{i=k_1+1}^m \mathbf{e}_i$ and define $\mathbf{J}_{ij} = \mathbf{u}_i \mathbf{u}_j^\top$ for $i, j \in [2]$. Then the population correlation matrix can be written as

$$\Gamma = \gamma_{12} \mathbf{J} + (\gamma_2 - \gamma_{12}) \mathbf{J}_{22} + (\gamma_1 - \gamma_{12}) \mathbf{J}_{11} + (1 - \gamma_1) \text{diag}(\mathbf{u}_1) + (1 - \gamma_2) \text{diag}(\mathbf{u}_2) \quad (1)$$

As the row sums for the first k_1 rows are the same (the same can be said for the last k_2 rows), the eigenvector should be of the form $\alpha \mathbf{u}_1 + \mathbf{u}_2$. By the definition,

$$\lambda(\alpha \mathbf{u}_1 + \mathbf{u}_2) = (\Gamma)(\alpha \mathbf{u}_1 + \mathbf{u}_2) = [(1 + (k_1 - 1)\gamma_1)\alpha + k_2\gamma_{12}] \mathbf{u}_1 + [k_1\gamma_{12}\alpha + (1 + (k_2 - 1)\gamma_2)] \mathbf{u}_2.$$

As the coefficients of \mathbf{u}_1 and \mathbf{u}_2 must agree in the left hand and right hand expressions, we can write

$$\begin{bmatrix} (1 + (k_1 - 1)\gamma_1) & k_2\gamma_{12} \\ k_1\gamma_{12} & (1 + (k_2 - 1)\gamma_2) \end{bmatrix} \begin{bmatrix} \alpha \\ 1 \end{bmatrix} = \lambda \begin{bmatrix} \alpha \\ 1 \end{bmatrix}$$

or equivalently,

$$\begin{bmatrix} (1 - \lambda + (k_1 - 1)\gamma_1) & k_2\gamma_{12} \\ k_1\gamma_{12} & (1 - \lambda + (k_2 - 1)\gamma_2) \end{bmatrix} \begin{bmatrix} \alpha \\ 1 \end{bmatrix} = 0.$$

The second row implies $\lambda = \alpha k_1 \gamma_{12} + 1 + (k_2 - 1)\gamma_2$, and substituting this into the first row gives us

$$k_1 \gamma_{12} \alpha^2 + ((k_2 - 1)\gamma_2 - (k_1 - 1)\gamma_1) \alpha - k_2 \gamma_{12} = 0.$$

The quadratic formula implies α can take on two values

$$\alpha = \frac{(k_1 - 1)\gamma_1 - (k_2 - 1)\gamma_2 \pm \sqrt{((k_1 - 1)\gamma_1 - (k_2 - 1)\gamma_2)^2 + 4k_1k_2\gamma_{12}^2}}{2k_1\gamma_{12}}$$

corresponding to the eigenvalues

$$\lambda = 1 + \frac{(k_1 - 1)\gamma_1 + (k_2 - 1)\gamma_2 \pm \sqrt{((k_1 - 1)\gamma_1 - (k_2 - 1)\gamma_2)^2 + 4k_1k_2\gamma_{12}^2}}{2}.$$

3 Computational Considerations for the eigenvector perturbation control chart

We specify the procedure to compute the leading eigenvector of \mathbf{R} .

Power iteration is a simple choice for computing the leading eigenvector of a symmetric matrix. A possible concern in using power iteration is the possibility of slow convergence, but we show this concern is negligible in the supplementary materials. We claim the dominance of the leading eigenvalue of \mathbf{R} over the rest of the eigenvalues results in fast convergence. Power iteration on \mathbf{R} converges geometrically with ratio λ_2/λ_1 , so slow convergence becomes an issue if $\lambda_2/\lambda_1 \approx 1$ (Ackleh, Allen, Kearfott, and Seshaiyer 2009, sec 5.2). As the eigenvalues of \mathbf{R} should not deviate greatly from the eigenvalues of $\mathbf{\Gamma}$, we can use $\tilde{\lambda}_2/\tilde{\lambda}_1$ to approximate convergence of power iteration on \mathbf{R} . It can be shown $\tilde{\lambda}_1 = 1 + \gamma_1(w - 1)$ and $\tilde{\lambda}_2 = \dots = \tilde{\lambda}_w = 1 - \gamma_1$. Therefore, $\tilde{\lambda}_2/\tilde{\lambda}_1 = \left(\frac{1+\gamma_1(w-1)}{1-\gamma_1}\right)^{-1} = \left(\frac{1}{1-\gamma_1} + \frac{\gamma_1}{1-\gamma_1}(w-1)\right)^{-1}$ which is well separated from 1 if either w is large or γ_1 is not too small. Note γ_1 is close to zero only if the in-control profile is difficult to distinguish from the noise (e.g., $\text{Var}[f] \leq \sigma^2$). We assume the in-control function f is sufficiently distinguishable from the noise, so we conclude that power iteration should converge reasonably quickly. Leveraging \mathbf{v} being close to $\frac{1}{\sqrt{w}}\mathbf{1}$ under in-control conditions, we adopt a modified version of power iteration from Iguchi, Mixon, Peterson, and Villar (2017) detailed in the Algorithm 1 which provides an early stopping rule when it becomes evident that the leading eigenvector is not $\frac{1}{\sqrt{w}}\mathbf{1}$.

Algorithm 1: Modified Power Iteration Detector (adapted from Iguchi et al. (2017))

```

Given: - Symmetric matrix  $\mathbf{M} \in \mathbb{R}^{w \times w}$ 
      - Unit eigenvector  $\tilde{\mathbf{v}} \in \mathbb{R}^w$ 
      - Tolerance:  $\zeta > 0$ 
Do:
Draw  $\mathbf{q}$  uniformly at random from the unit sphere in  $\mathbb{R}^w$ 
while TRUE
    if  $|\mathbf{q}^\top \mathbf{M} \mathbf{q}| > |\tilde{\mathbf{v}}^\top \mathbf{M} \tilde{\mathbf{v}}|$  ##  $\tilde{\mathbf{v}}$  is not the leading eigenvector of  $\mathbf{M}$ 
        return( $\mathbf{q}$ ); break
    else if  $(\tilde{\mathbf{v}}^\top \mathbf{q})^2 \geq 1 - \zeta$  ##  $\tilde{\mathbf{v}}$  and  $\mathbf{q}$  are close enough
        return( $\mathbf{q}$ ); break
    end
     $\mathbf{q} = \mathbf{M} \mathbf{q} / \|\mathbf{M} \mathbf{q}\|_2$ 
end

```

4 The eigenvector perturbation control chart

Leveraging predictors being fixed for all t , we perform a parametric bootstrap to compute a control limit. The procedure for this parametric bootstrap is outlined below for large values of N and N_0 with $N_0 \gg N$. Once a control limit is in hand, the Eigenvector Perturbation Control Chart (Algorithm 2) can be executed.

1. Compute $\hat{f}(\mathbf{X}) = \frac{1}{m} \sum_{t=1-m}^0 \mathbf{y}^t$ and $\hat{\sigma}^2 = \frac{1}{n(m-1)} \sum_{i=1}^n \sum_{t=1-m}^0 (\mathbf{y}_i^t - \hat{f}(\mathbf{X})_i)^2$.
2. Compute $\mathbf{y}_*^s = \hat{f}(\mathbf{X}) + \boldsymbol{\epsilon}_*^s$ for all $s \in [N_0]$ where $\boldsymbol{\epsilon}_*^s \sim N(0, \hat{\sigma}^2 \mathbf{I})$
3. For every $l \in [N]$, compute a sample correlation matrix \mathbf{R}_l using w of the \mathbf{y}_*^s sampling without replacement.
4. Compute $S_l = \max_{k_1 \in K} \|\mathbf{v}(k_1) - \frac{1}{\sqrt{w}} \mathbf{1}\|_2$ for every bootstrapped correlation matrix \mathbf{R}_l .
5. Using a small $c > 0$, set $U = F(1 - c; \hat{\mu}_S, \hat{\sigma}_S^2)$ where F is a normal distribution function for with mean $\hat{\mu}_S$ and variance $\hat{\sigma}_S^2$ and where these estimates are the typical unbiased estimators for the mean and variance of the $\{S_l\}_{l \in [N]}$ in the previous step.

5 An illustration of distinct but dependent predictors with the eigenvector perturbation control chart

In the main manuscript, we use a common fixed design for the predictors even though we only require the predictors to be dependent between time points (see section 2.1). We take a moment to illustrate how this can be relaxed. To illustrate this, see Figure 1 which is produced from a small simulation study. For each value of n , 500 trials are conducted wherein

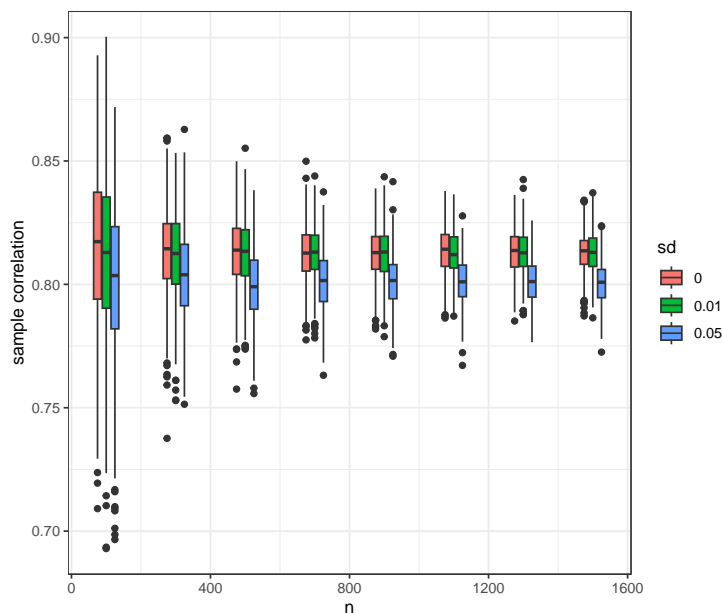


Figure 1: Distribution of sample correlations after perturbation of design points

each trial a set of x_1, \dots, x_n design points are generated from a uniform(0,1) distribution and then another set of design points x_1^*, \dots, x_n^* are obtained by adding $N(0, \text{sd})$ noise to the design points x_1, \dots, x_n . The profiles are of the form $y_i = 7x_i^2 + \epsilon_i$ for $i \in [n]$ and $\epsilon \sim N(0, 1)$. We then compute the sample correlation of the responses from the profile using the design points x_1, \dots, x_n with the responses from the profile using the design points x_1^*, \dots, x_n^* . Observe in Figure 1 that although the sample correlations seem to converge to different values, they do converge.

Ultimately, we care more about the variability of the sample correlation of two profiles. The goal of the control chart is to make the appropriate block structure as demonstrated in Figure 1 of the main manuscript as clear as possible. If the variability of the sample correlations is large, then it becomes less apparent both to the eye when viewing a heatmap of \mathbf{R} and to the eigenvector perturbation control chart. See the Figure 2 below for a demonstration of this concept. In Figure 2, each sub-figure is obtained by first fixing a set of design points. Then 40 observed profiles are generated by first perturbing the design points then inputting the design points into either the in-control function or the out-of-control function and lastly $N(0, 1)$ noise is added. In the figure above we see as we increase the perturbation of the design points the “one-block” structure of the correlation matrix becomes less apparent. In the middle row, we fix the perturbation standard deviation to be 0.25 to match Figure 1e. Notice the one block structure is regained at the cost of the sample correlations being smaller in magnitude. The last row uses an out of control profile of $y_i = 3x_i^2 - x_i + \epsilon_i$. Observe using the same values of n as in the middle row allows us to recover a clear two block structure. Therefore, our control chart can handle design points

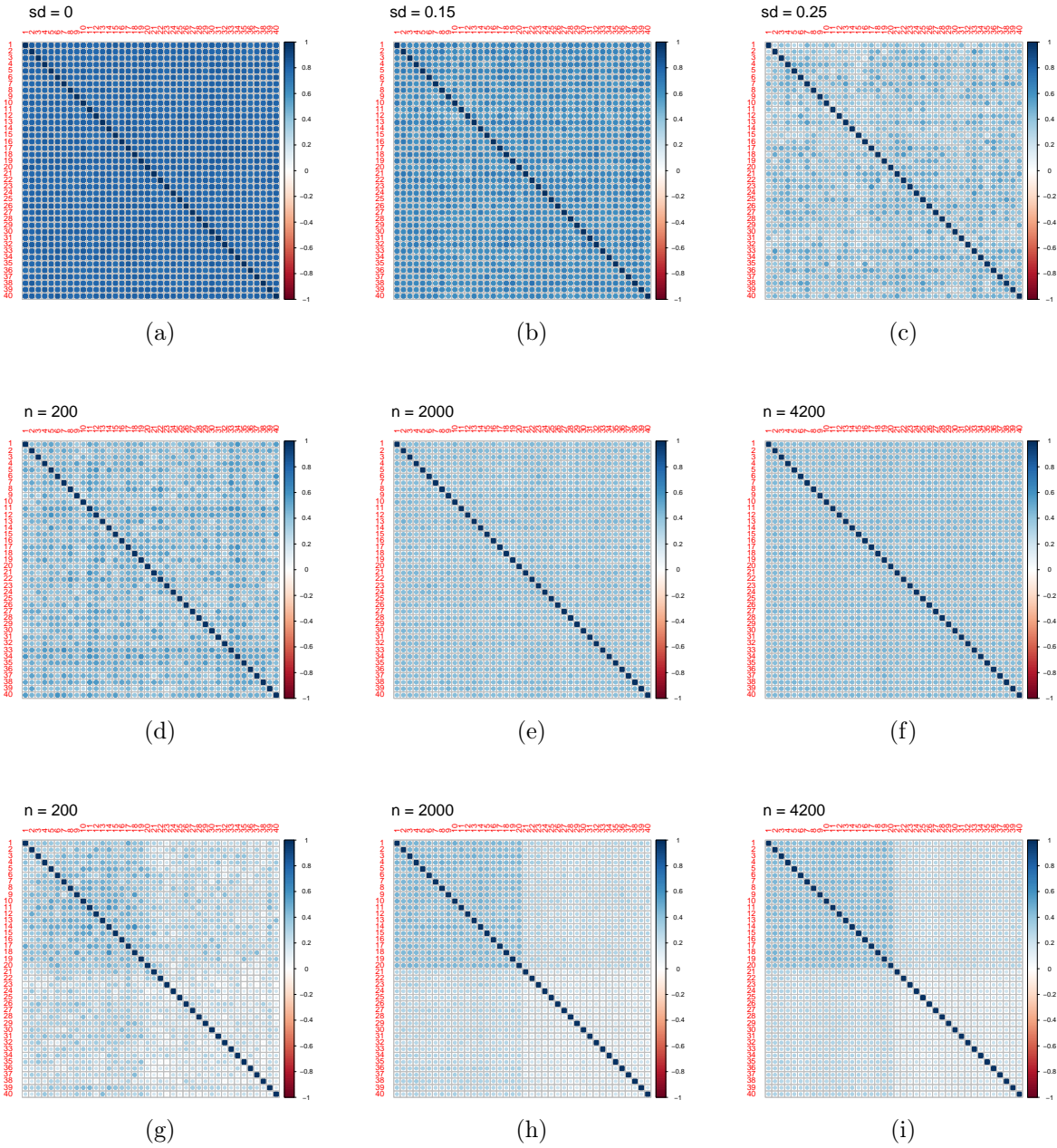


Figure 2: A demonstration of how increasing n can overcome perturbation of design points between profiles. (Top row) From left to right the standard deviation of the perturbation increases for IC profiles. (Middle row) From left to right the profile sample size n increases and all 40 profiles are IC. (Bottom row) From left to right the profile sample size n increases and the first 20 profiles are IC and the last 20 profiles are OOC.

changing over time so long as they are dependent.

6 Details regarding the simulation study comparing the proposed control chart to its competitors with multiple predictors

The factors and levels of the full factorial design of the comparative simulation study are detailed in Table 1. The values of the convex combination parameter ν are taken from Iguchi et al. (2021) and are shown in Table 2. To justify the lower bound of 7×10^6 for the ARL_0 of the proposed control chart for the profile combinations listed in Table 1, the proposed control chart was run until either timestep 10^7 or a false alarm occurred. The results of carrying out this experiment over 100 trials for each in-control profile yield lower bounds on the ARL_0 and are listed in Table 3. Computational speed was also measured across the profile monitoring methods being considered and the results are shown in Table 4.

The SVR approach from Li et al. (2019) used a smoothing parameter λ in their EWMA based scheme and performed a sensitivity analysis for this parameter. They observed that ARL_1 becomes shorter as λ becomes smaller. We used the smallest value ($\lambda = 0.05$) from their sensitivity analysis. Li et al. (2019) recommended basing the monitoring statistic using the 2nd, 3rd, or 5th Williams et al. (2007) statistics. As described in Iguchi et al. (2021), the performance of the SVR approaches on the profile combinations in their simulation study do not differ greatly in ARL_1 . As the 5th such statistic resulted in the smallest FAR for the SVR approach in Iguchi et al. (2021), we also use this statistic for the SVR approach.

For calibrating control limits using a Monte Carlo approach, control limits were calibrated to a target ARL_0 of 200 or 370 using f explicitly to generate profiles. Each trial in the Monte Carlo approach consisted of randomly generating a set of historical profiles, fitting a model to the historical profiles, and monitoring a sequence of in-control profiles until a false alarm was raised. Control limits were calibrated by finding the smallest observed monitoring statistic that met or exceeded the desired ARL_0 over 390 trials. When the bootstrap approach to setting a control limit is used in the eigenvector perturbation control chart, settings of $\zeta = 10^{-3}$, $c = 10^{-14}$, $N = 1000$, and $N_0 = 5000$ were used.

Table 1: The factor and levels of the simulation study. The values of ν were obtained from Iguchi et al. (2021) where they calibrated $\nu \in (0, 1)$ to achieve a particular SNR.

Factor	Levels
In-control & out-of-control functions	$- f(\mathbf{x}) = 1 + 3x_1 + 2x_2 + x_3$ $- f(\mathbf{x}) = \frac{4}{9}(3x_1 + 2x_2 + x_3)^2$ $- f(\mathbf{x}) = 1 + 3x_1 + 2x_2 + x_3$ $- f(\mathbf{x}) = \frac{4}{9}(3x_1 + 2x_2 + x_3)^2$
	$h(\mathbf{x}) = \nu f(\mathbf{x}) + (1 - \nu) \sin(2\pi x_1 x_2)$ $h(\mathbf{x}) = \nu f(\mathbf{x}) + (1 - \nu) 5 \sin(2\pi x_1 x_2)$ $h(\mathbf{x}) = \nu f(\mathbf{x}) + (1 - \nu) 25 x_1 - 0.5 e^{-x_2} I(x_3 > 0.5)$ $h(\mathbf{x}) = \nu f(\mathbf{x}) + (1 - \nu) 25 x_1 - 0.5 e^{-x_2} I(x_3 > 0.5)$
Change point detector	- Li et al. (2019) detector with the 5th Williams et al. (2007) statistic - Iguchi et al. (2021) - Eigenvector Perturbation Control Chart
SNR	3, 5

Algorithm 2: Eigenvector Perturbation Control Chart

Given: – Historical data: $\mathbf{X}^t, \mathbf{y}^t$ where $\mathbf{y}^t \in \mathbb{R}^n$, $\mathbf{X}^t \in \mathbb{R}^{n \times p}$, $t \in \{1 - m, \dots, 0\}$
– Upper control limit: $U > 0$
– A nonempty $K \subset [w - 1]$
– Tolerance for power iteration detector: ζ
– Window size: $w \leq m$

Do:
Compute the sample correlation matrix $\mathbf{R}^* \in \mathbb{R}^{m \times m}$ of the historical profiles.
Set \mathbf{R} to be the last w columns and rows of \mathbf{R}^*
 $S = -1$; $T = 1$
#Conduct process monitoring
while $S < U$
 Observe $\mathbf{y}^T \in \mathbb{R}^n$; update \mathbf{R} to reflect correlations of $\{\mathbf{y}^{T-w+1}, \dots, \mathbf{y}^T\}$
 for every k_1 in K
 if $T < w - k_1$, set $\mathcal{I} = [m - w + k_1 + T]$ **else** set $\mathcal{I} = [m]$
 Sample k_1 indices j_1, \dots, j_{k_1} from \mathcal{I} without replacement; set $\mathbf{R}(k_1) = \mathbf{R}$
 Replace the first k_1 rows/columns of $\mathbf{R}(k_1)$ with the j_1, \dots, j_{k_1} rows/columns of \mathbf{R}^*
 $\mathbf{v}(k_1) = \text{modified_power_iteration_detector}\left(\mathbf{R}(k_1), \frac{1}{\sqrt{w}}\mathbf{1}, \zeta\right)$
 $S = \max_{k_1 \in K} \|\mathbf{v}(k_1) - \frac{1}{\sqrt{w}}\mathbf{1}\|_2$
 if $S > U$, claim change point occurred **else** set $T = T + 1$

Table 2: Values v for a targeted signal-to-noise ratio

f^0	h	SNR		
		3	5	7
Linear	Sinusoid	0.45676033	0.29857462	0.16998640
	Non-differentiable	0.39454966	0.21840187	0.07522249
Nonlinear	Sinusoid	0.46154345	0.30484461	0.17747209
	Non-differentiable	0.5465315	0.4146351	0.3074320

Table 3: ARL_0^* of eigenvector perturbation control charts with 10^{-14} quantile trick using equally spaced k_1^* on profiles from Table 1. Due to memory and time constraints, we compute a right censored average run length ARL_0^* taken over runs that raised a false alarm by timestep 10^7 (and excludes runs having no false alarms by timestep 10^7). As the earliest a false alarm could have been raised for the censored trials is $10^7 + 1$, we can place a lower bound on ARL_0 by assuming the censored trials all raised an alarm at time step $10^7 + 1$.

In-control profile	m	ARL_0^*	Finished by $T = 10^7$	Lower bound on ARL_0
quadratic	20	3947093	35	7881483
linear	20	2553138	37	7244662
quadratic	40	4362645	29	8365168
linear	40	2815431	52	7068576

Table 4: Runtimes in seconds for 100 iterations of computing the monitoring statistic from an observed profile and deciding if a profile is in-control or out-of-control. The simulations were conducted under $m = 20$ historical profiles, a window size of $w = 10$ (if applicable), and the profile used for all 100 iterations was the in-control quadratic profile from Table 1, and $m = 20$.

Method	Min	Median	Max
Eigenvector Perturbation	0.000	0.001	0.060
Li et al. (2019)	0.021	0.025	0.041
Iguchi et al. (2021)	15.452	28.003	41.365

Table 5: The factors and levels for the simulation study on the eigenvector perturbation control chart using quadratic polynomials for the in-control and out-of-control profiles. All possible treatment combinations were implemented. Note certain combinations of $\text{Var}[f]$, SNR, $\rho(f, h)$ and choice of convexity cannot be achieved.

Factor	Level
τ	0, 30, 10^4
n	128, 256, 512
m	20, 40
m/w	1, 2
SNR	3, 5
$\text{Var}[f]$	2,4,6
$\rho(f, h)$	0.75, 0.9
convexity of h with respect to f and g	convex, non-convex combinations

7 Details regarding the simulation study using quadratic in-control and out-of-control profiles

If $\nu \in (0, 1)$, then h is a convex combination of f and g . Otherwise, h is a nonconvex combination of f and g . We additionally constrain g such that $\text{Cov}[f, g] = 0$ to ease profile calibration efforts and improve interpretability of the results. Observe if $\nu < 0$, then $\rho(f, h) < 0$. As we want to consider difficult cases for the eigenvector perturbation control chart we will ignore the scenario where $\nu < 0$.

Recall the eigenvector perturbation of $\mathbf{\Gamma}$ is a function of γ_1 , γ_{12} , and γ_2 . Although these are biased estimates of their population counterparts, they converge to the population correlation as $n \rightarrow \infty$. As such, we provide an illustration for the population correlations for two in-control profiles $\rho(f + \epsilon_1, f + \epsilon_2)$, for an in-control profiles and an out-of-control profile $\rho(f + \epsilon_1, h + \epsilon_2)$, and for two out-of-control profiles $\rho(h + \epsilon_1, h + \epsilon_2)$ for all possible profile combinations in Table 5, where $\epsilon_1, \epsilon_2 \in \mathbb{R}$ are noise independent of each other and of the predictors \mathbf{x} . The quantities are computed as

$$\rho(f + \epsilon_1, f + \epsilon_2) = \frac{\text{Var}[f]}{\text{Var}[f] + \sigma^2}, \quad \rho(h + \epsilon_1, h + \epsilon_2) = \frac{\text{Var}[h]}{\text{Var}[h] + \sigma^2},$$

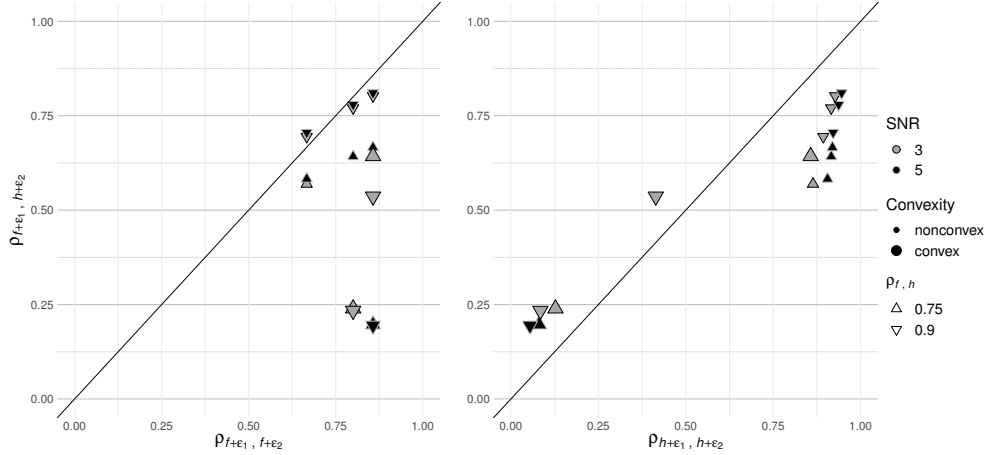


Figure 3: A visualization of the population correlation between profile combinations in Table 5. Each point corresponds to a particular treatment combination of an in-control profile and an out-of-control profile in Table 5

and

$$\rho(f + \epsilon_1, h + \epsilon_2) = \frac{\text{Cov}[f, h]}{\sqrt{\text{Var}[f] + \sigma^2} \sqrt{\text{Var}[h] + \sigma^2}} = \rho(f, h) \rho(f + \epsilon_1, f + \epsilon_2)^{1/2} \rho(h + \epsilon_1, h + \epsilon_2)^{1/2}$$

where the last equality is obtained through repeated uses of the definition of correlation.

There is a counterintuitive result: the ARL_1 did not decrease uniformly with increasing SNR and $\text{Var}[f]$ (e.g., $\text{Var}[f] = 4$). This curious result is explained by considering the correlation between *profiles* as opposed to the correlation between in-control and out-of-control functions f and h . As Figure 3 shows, the out-of-control profiles obtained through a nonconvex combination of f and g tend to have $\rho(f + \epsilon_1, f + \epsilon_2) \approx \rho(f + \epsilon_1, h + \epsilon_2)$. In fact, the closer these two quantities are, the larger the ARL_1 . It seems the only reason the eigenvector perturbation control chart is able to detect an out-of-control profile is due to the difference between $\rho(h + \epsilon_1, h + \epsilon_2)$ and $\rho(f + \epsilon_1, h + \epsilon_2)$. This scenario should be difficult for any control chart that monitors correlations.

8 Details regarding competitors omitted from section 4.2.2

We compare two other profile monitoring methods which face computational difficulties in this simulation study. Qiu et al. (2010) conjecture their iterative method for estimating a profile does not face convergence issues if both m and n are sufficiently large. They recommend values of $n \geq 20$ and $m \geq 500$. We attempted to see if this method could still estimate an in-control profile with $m = 40$ historical, in-control profiles. We attempted estimation 100 times, with each attempt using a different set of $m = 40$ profiles, and failed to converge 98 times. If their approach fails to estimate the IC function, monitoring cannot occur.

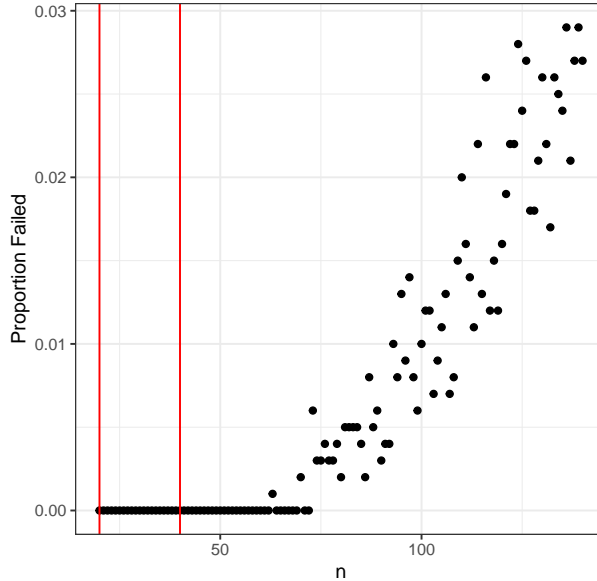


Figure 4: Proportion of times the control chart of Zou et al. (2008) creates an ill-defined monitoring statistic. Red lines correspond to values of n used in the original manuscript.

Similarly, Zou et al. (2008) ran into a computational issue for $n > 63$ where we used $n = 128$ in section 4.2.2 of the main manuscript. We were unable to compare the performance of this method in terms of ARL_1 and False Alarm Rates with our proposed method, and we provide more detail here than in the main manuscript. Their method ran into a computational issue for $n > 63$ where we used $n = 128$ in the simulation study in section 4.2.2. Their approximation of a particular density results in a non-finite estimate of σ^2 which results in an ill-defined monitoring statistic. Specifically, the estimate (using the notation of Zou et al. (2008)) $\tilde{\sigma}_j = \Phi^{-1}(\psi(n\hat{\sigma}_j^2))$ is equal to $-\infty$ when $\psi(n\hat{\sigma}_j^2) = 0$. The function ψ is the distribution function of the quantity $n\hat{\sigma}_j^2$ which they approximate using the method of Imhoff (1961). The probability of this approximation incorrectly stating the cumulative probability is zero increases with n . Figure 4 demonstrates how often this event occurred as a function of n . In Figure 4, for each value of n , 10^3 trials were performed wherein each trial the predictors were equispaced (see section 3 of Zou et al. (2008)), a profile is randomly generated, and the estimate of $\tilde{\sigma}_j$ was computed. This causes an issue as their monitoring statistic requires the multiplication of 0 with $\tilde{\sigma}_j$, which is ill-defined when $\tilde{\sigma}_j = -\infty$. We note that this issue was not addressed in Zou et al. (2008) as they used values of $n = 20, 40$ in their simulation studies, which are shown in red lines in the above figure. So we claim the EP control chart is preferable, provided n is sufficiently large.

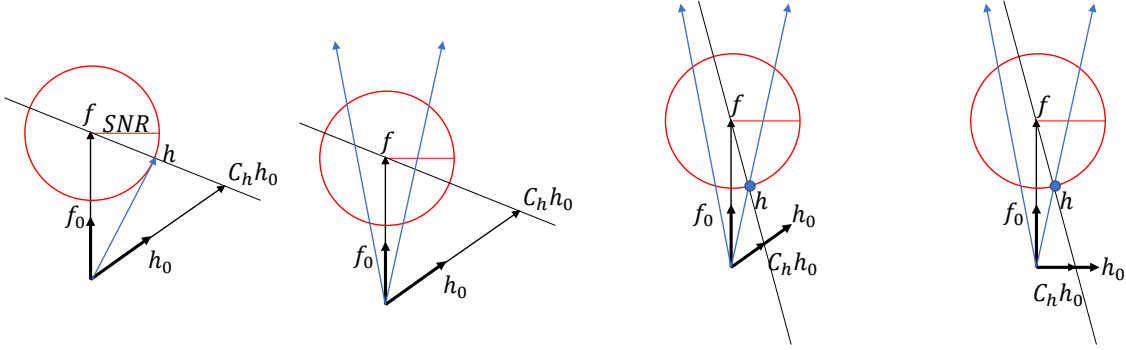


Figure 5: Visualizing profile calibration in a functional space. (left) Calibrating in-control and out-of-control profiles without the correlation constraint. The ν parameter is chosen to achieve a desired SNR. (middle left) Blue lines correspond to a cone of functions with correlation no less than the desired $\rho(f, h)$. Observe adding the correlation constraint requires adjusting C_h in addition to ν . (middle right) An out-of-control h denoted by the blue dot is calibrated to a specified the desired $\text{Var}[\delta]$, $\text{Var}[f]$, $\rho(f, h)$. Also observe in this instance, there are two values of ν possible. The choice of $\nu \in (0, 1)$ is shown, where $\nu > 1$ would correspond to h lying on the upper left portion of the circle of radius SNR in the figure. (right) A visualization of the proposed calibration approach for h using orthogonal f_0 and h_0 .

9 A general approach to profile calibration

9.1 A more general setup

In profile monitoring, we are provided with an in-control profile f or samples from f . In a computer experiment, we need to define f first and then define some different out-of-control function h . Certainly, this could be picked arbitrarily, but we wish to calibrate h to such that certain notions of “difference” between f and h are met. We retain a signal-to-noise ratio defined as $\sigma_{\text{signal}}^2 = \text{Var}[f - h] / \text{Var}[\epsilon]$ as one of such notions. There are, however, an infinite number of such h that can meet such a requirement as can be seen by considering a ball of radius σ_{signal} with respect to a norm defined by $\|h\|_2^2 = \text{Var}[h]$. We add further notions of difference which are relevant to the eigenvector perturbation control chart. If $h \neq f$, then h must be different in some orthogonal direction to f . Let h_0 be a function of unit norm in this orthogonal direction. Then we can define h to be an affine combination of f and $C_h h_0$ for some $C_h > 0$. That is, $h = \nu f + (1 - \nu)C_h h_0$. As the eigenvector perturbation control chart monitors correlations, we will also add the correlation between f and h , denoted $\rho(f, h)$ as another constraint. For similar reasoning, we add $\text{Var}[f]$ as a constraint on the choice of f as the sample correlation of two observed in-control profiles becomes more stable as $\text{Var}[f] / \text{Var}[\epsilon]$ becomes larger. To accommodate this calibration parameter, we pick some function f_0 to be a scaled version of f with unit norm. In summary, the more general set

up for calibrating profiles is below.

$$\begin{aligned}
&\text{In-control function: } f = C_f f_0 \\
&\text{Out-of-control function: } h = \nu f + (1 - \nu)C_h h_0 \\
&\text{“signal”}: \delta = f - h = (1 - \nu)(C_f f_0 - C_h h_0)
\end{aligned} \tag{2}$$

The choices of f_0, h_0 can be taken from some random linear combination of basis functions (such that $\text{Cov}[f_0, h_0] = 0$). Now the task is given $f_0, h_0, \text{Var}[f], \text{Var}[\delta]$, and $\rho(f, h)$, find ν, C_f , and C_h .

Finding C_f follows from the definition of f_0 :

$$C_f = \sqrt{\text{Var}[f]}.$$

We introduce the following lemma which demonstrates ways of finding ν and C_h .

Lemma 1 (Identities for computing ν and C_h). *Under the setting in Eq (2) and assuming $C_h > 0$ WLOG, the following identities hold:*

- (ν as a function of C_h): $\nu = 1 \pm \sqrt{\frac{\text{Var}[\delta]}{\text{Var}[f] + C_h^2}}$
- (C_h as a function of ν): $C_h = \sqrt{\frac{\text{Var}[\delta]}{(1-\nu)^2} - \text{Var}[f]}$.
- ($\rho(f, h)$ and ν share the same sign): $\rho(f, h) = \frac{\nu}{\sqrt{2\nu-1 + \frac{\text{Var}[\delta]}{\text{Var}[f]}}}$
- (ν as a function of $\rho(f, h)$): $\nu = \rho(f, h)^2 \pm \sqrt{\rho(f, h)^4 + \rho(f, h)^2 \left(\frac{\text{Var}[\delta]}{\text{Var}[f]} - 1 \right)}$.

Proof. As $\text{Var}[\delta] = (1 - \nu)^2 \text{Var}[f - C_h h_0]$, and $\text{Cov}[f, h_0] = 0$ by design,

$$\text{Var}[\delta] = (1 - \nu)^2(\text{Var}[f] + C_h^2 \text{Var}[h_0]),$$

and

$$(1 - \nu)^2 = \frac{\text{Var}[\delta]}{\text{Var}[f] + C_h^2 \text{Var}[h_0]}. \tag{3}$$

Therefore,

$$\nu = 1 \pm \sqrt{\frac{\text{Var}[\delta]}{\text{Var}[f] + C_h^2 \text{Var}[h_0]}} \tag{4}$$

which is solely a function of C_h . By the definition of correlation and the construction of

orthogonal f_0 and h_0 ,

$$\begin{aligned}
\rho(f, h) &= \frac{\text{Cov}[f, h]}{\sqrt{\text{Var}[f] \text{Var}[h]}} \\
&= \frac{\text{Cov}[f, \nu f + (1 - \nu)C_h h_0]}{\sqrt{\text{Var}[f] \text{Var}[h]}} \\
&= \frac{\nu \text{Var}[f] + (1 - \nu)C_h \text{Cov}[f, h_0]}{\sqrt{\text{Var}[f] \text{Var}[h]}} \\
&= \frac{\nu \text{Var}[f]}{\sqrt{\text{Var}[f] \text{Var}[h]}} \\
&= \nu \sqrt{\frac{\text{Var}[f]}{\text{Var}[h]}} \\
&= \nu \sqrt{\frac{\text{Var}[f]}{\nu^2 \text{Var}[f] + (1 - \nu)^2 C_h^2 \text{Var}[h_0]}} \\
&= \frac{\nu}{\sqrt{\nu^2 + (1 - \nu)^2 C_h^2 \frac{\text{Var}[h_0]}{\text{Var}[f]}}}.
\end{aligned}$$

Rewriting Eq. (3) as

$$C_h^2 = \frac{1}{\text{Var}[h_0]} \left(\frac{\text{Var}[\delta]}{(1 - \nu)^2} - \text{Var}[f] \right).$$

Substituting this expression into the last formulation of $\rho(f, h)$ gives

$$\rho(f, h) = \frac{\nu}{\sqrt{\nu^2 + \frac{\text{Var}[\delta]}{\text{Var}[f]} - (1 - \nu)^2}} = \frac{\nu}{\sqrt{2\nu - 1 + \frac{\text{Var}[\delta]}{\text{Var}[f]}}}. \quad (5)$$

We can rewrite Eq. (5) as a quadratic in ν to obtain an expression of ν in terms of $\rho(f, h)$:

$$\nu^2 - 2\rho(f, h)^2 + \rho(f, h)^2 \left(1 - \frac{\text{Var}[\delta]}{\text{Var}[f]} \right).$$

The roots of the quadratic after some simplification are

$$\nu = \rho(f, h)^2 \pm \sqrt{\rho(f, h)^4 + \rho(f, h)^2 \left(\frac{\text{Var}[\delta]}{\text{Var}[f]} - 1 \right)}. \quad (6)$$

□

Note that there may be two choices of ν, C_h , which can achieve the same calibration. It turns out the behavior of $\rho(f, h)$ as a function of C_h can be classified into three cases illustrated in Figure 6. In the cases where $\text{Var}[f] \leq \text{Var}[\delta]$, the horizontal asymptote (which happens to be $1/\sqrt{1 + \text{Var}[\delta]/\text{Var}[f]}$) dictates which root to use to achieve a desired correlation. In the case where $\text{Var}[f] > \text{Var}[\delta]$, correlations above the asymptote can be achieved using either root in Eq. (4). Additionally, observe when $\text{Var}[f] \geq \text{Var}[\delta]$ there and there exists a minimum achievable correlation. As a result of the discriminant in (6) being positive, the minimum achievable correlation when $\text{Var}[f] > \text{Var}[\delta]$ is $\sqrt{1 - \frac{\text{Var}[\delta]}{\text{Var}[f]}}$.

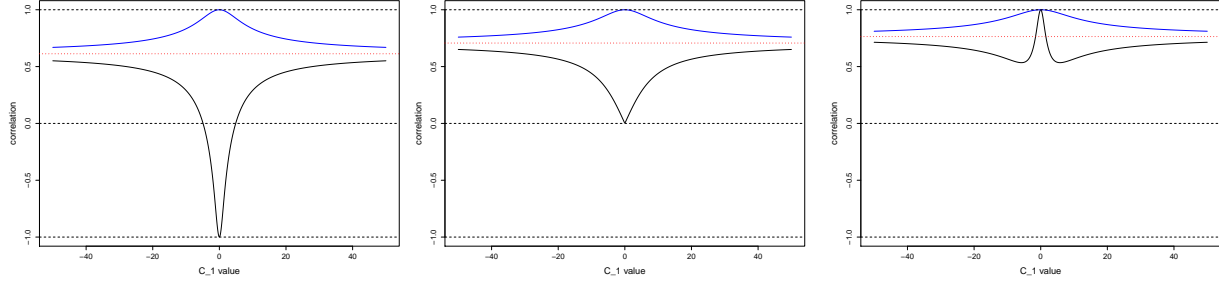


Figure 6: A plot of $\rho(f, h)$ as a function of C_h . The top blue line corresponds to the positive root in the expression for ν in Eq. (4). The bottom black line corresponds to the negative root. The horizontal red dotted line corresponds to the horizontal asymptote of $\rho(f, h)(C_h)$. In each plot, $\text{Var}[\delta] = 5$. Moving from left to right, the values of $\text{Var}[f]$ are 3, 5, and 7.

9.2 Calibrating for linear and quadratic polynomial profiles

Here we assume f_0 and h_0 are of the following form:

$$\begin{aligned} f_0(\mathbf{x}) &= \mathbf{x}^\top \mathbf{A} \mathbf{x} + \mathbf{a}^\top \mathbf{x} \\ h_0(\mathbf{x}) &= \mathbf{x}^\top \mathbf{B} \mathbf{x} + \mathbf{b}^\top \mathbf{x} \end{aligned}$$

We can randomly pick f_0 but the choice of h_0 will depend on the choice of f_0 (in that $\text{Cov}[f_0, h_0] = 0$). Additionally, normalizing a random choice of quadratic polynomial to obtain f_0 will require us to compute $\text{Var}[f_0]$. In order to quickly calibrate profiles, we will need a fast computation of the covariance. The covariance between f_0 and h_0 can be written as

$$\begin{aligned} \text{Cov}[f_0, h_0] &= \text{Cov}[\mathbf{x}^\top \mathbf{A} \mathbf{x} + \mathbf{a}^\top \mathbf{x}, \mathbf{x}^\top \mathbf{B} \mathbf{x} + \mathbf{b}^\top \mathbf{x}] \\ &= \text{Cov}[\mathbf{x}^\top \mathbf{A} \mathbf{x}, \mathbf{x}^\top \mathbf{B} \mathbf{x}] + \text{Cov}[\mathbf{x}^\top \mathbf{A} \mathbf{x}, \mathbf{b}^\top \mathbf{x}] + \text{Cov}[\mathbf{a}^\top \mathbf{x}, \mathbf{x}^\top \mathbf{B} \mathbf{x}] + \text{Cov}[\mathbf{a}^\top \mathbf{x}, \mathbf{b}^\top \mathbf{x}]. \end{aligned} \tag{7}$$

We handle each term in turn, in reverse order. The last term can be written as

$$\text{Cov}[\mathbf{a}^\top \mathbf{x}, \mathbf{b}^\top \mathbf{x}] = \mathbf{a}^\top \mathbf{b} / 12$$

and the middle terms can be written

$$\begin{aligned} \text{Cov}[\mathbf{x}^\top \mathbf{A} \mathbf{x}, \mathbf{b}^\top \mathbf{x}] &= \frac{1}{24} \mathbf{1}^\top (\mathbf{A} + \mathbf{A}^\top) \mathbf{b} \quad \text{and} \\ \text{Cov}[\mathbf{a}^\top \mathbf{x}, \mathbf{x}^\top \mathbf{B} \mathbf{x}] &= \frac{1}{24} \mathbf{1}^\top (\mathbf{B} + \mathbf{B}^\top) \mathbf{a}. \end{aligned}$$

WLOG we show the first identity with the following calculation:

$$\begin{aligned}
\text{Cov}[\mathbf{x}^\top \mathbf{A} \mathbf{x}, \mathbf{a}^\top \mathbf{x}] &= \text{Cov} \left(\sum_{i,j} A_{ij} X_i X_j, \sum_k a_k X_k \right) \\
&= \sum_{i,j,k} A_{ij} a_k \text{Cov}[X_i X_j, X_k] \\
&= \sum_{i=k \neq j} A_{ij} a_k \mathbb{E}[X_j] \text{Var}[X_i] + \sum_{j=k \neq i} A_{ij} a_k \mathbb{E}[X_j] \text{Var}[X_i] + \sum_i A_{ii} a_i \text{Cov}[X_i^2, X_i] \\
&= \frac{1}{24} \sum_{i=k \neq j} A_{ij} a_k + \frac{1}{24} \sum_{j=k \neq i} A_{ij} a_k + \frac{1}{12} \sum_i A_{ii} a_i \\
&= \frac{1}{24} \left(\sum_{ij} A_{ij} a_i + \sum_{ij} A_{ij} a_j \right) \\
&= \frac{1}{24} \mathbf{1}^\top (\mathbf{A} + \mathbf{A}^\top) \mathbf{a}.
\end{aligned}$$

The first term in (7) is rather complicated and is the reason why calculating $\text{Var}(f)$ is slow for a quadratic profile. The lemma below gives the expression for this term.

Lemma 2. *Let $\mathbf{x} = (X_1, \dots, X_d)^\top \sim \text{Unif}([0, 1]^d)$ with independent components. Then for \mathbf{A}, \mathbf{B} defined above,*

$$\begin{aligned}
\text{Cov}[\mathbf{x}^\top \mathbf{A} \mathbf{x}, \mathbf{x}^\top \mathbf{B} \mathbf{x}] &= \mathbb{E}[\mathbf{x}^\top \mathbf{A} \mathbf{x} \mathbf{x}^\top \mathbf{B} \mathbf{x}] - \mathbb{E}[\mathbf{x}^\top \mathbf{A} \mathbf{x}] \mathbb{E}[\mathbf{x}^\top \mathbf{B} \mathbf{x}] \\
&= \frac{1}{2^4} \sum_{i,j,k,l \text{ distinct}} A_{ij} B_{kl} + \frac{1}{6} \sum_{3 \text{ distinct } i,j,k,l} A_{ij} B_{kl} + \frac{1}{3^2} \sum_{\substack{2 \text{ distinct } i,j,k,l \\ \text{each of size } 2}} A_{ii} B_{kl} \\
&\quad + \frac{1}{2 \cdot 4} \sum_{\substack{2 \text{ distinct } i,j,k,l \\ \text{one of size } 1 \text{ the other of size } 3}} A_{ii} B_{kl} + \frac{1}{5} \sum_i A_{ii} B_{ii} \\
&\quad - \left(\frac{1}{12} \text{tr}(\mathbf{A}) + \frac{1}{4} \mathbf{1}^\top \mathbf{A} \mathbf{1} \right) \left(\frac{1}{12} \text{tr}(\mathbf{B}) + \frac{1}{4} \mathbf{1}^\top \mathbf{B} \mathbf{1} \right). \tag{8}
\end{aligned}$$

Proof. By a well known identity,

$$\text{Cov}[\mathbf{x}^\top \mathbf{A} \mathbf{x}, \mathbf{x}^\top \mathbf{B} \mathbf{x}] = \mathbb{E}[\mathbf{x}^\top \mathbf{A} \mathbf{x} \mathbf{x}^\top \mathbf{B} \mathbf{x}] - \mathbb{E}[\mathbf{x}^\top \mathbf{A} \mathbf{x}] \mathbb{E}[\mathbf{x}^\top \mathbf{B} \mathbf{x}].$$

By taking the bilinear form of $\mathbf{x}^\top \mathbf{A} \mathbf{x}$ we can compute its expectation.

$$\begin{aligned}
\mathbb{E}[\mathbf{x}^\top \mathbf{A} \mathbf{x}] &= \mathbb{E} \left[\sum_{i,j} A_{ij} X_i X_j \right] \\
&= \mathbb{E} \left[\sum_{i,j} A_{ij} X_i X_j \right] \\
&= \sum_i A_{ii} \mathbb{E} \left[X_i^2 + \sum_{i \neq j} A_{ij} \right] \mathbb{E}[X_i] \mathbb{E}[X_j] \\
&= \sum_i A_{ii} \left(\frac{1}{12} + \frac{1}{4} \right) + \sum_{i \neq j} A_{ij} \frac{1}{4} \\
&= \frac{1}{12} \text{tr}(\mathbf{A}) + \frac{1}{4} \mathbf{1}^\top \mathbf{A} \mathbf{1}
\end{aligned}$$

A similar result holds for \mathbf{B} . Now we need an expression for $\mathbb{E}[\mathbf{x}^\top \mathbf{A} \mathbf{x} \mathbf{x}^\top \mathbf{B} \mathbf{x}]$. Using the fact that $\mathbf{x}^n \sim \text{Beta}(1/n, 1)$, we can write

$$\begin{aligned}
\mathbb{E}[\mathbf{x}^\top \mathbf{A} \mathbf{x} \mathbf{x}^\top \mathbf{B} \mathbf{x}] &= \mathbb{E} \left[\left(\sum_{i,j} X_i A_{ij} X_j \right) \left(\sum_{k,l} X_k B_{kl} X_l \right) \right] \\
&= \sum_{i,j,k,l} A_{ij} B_{kl} \mathbb{E}[X_i X_j X_k X_l] \\
&= \frac{1}{2^4} \sum_{i,j,k,l \text{ distinct}} A_{ij} B_{kl} + \frac{1}{6} \sum_{3 \text{ distinct } i,j,k,l} A_{ij} B_{kl} + \frac{1}{3^2} \sum_{\substack{2 \text{ distinct } i,j,k,l \\ \text{each of size 2}}} A_{ii} B_{kl} \\
&\quad + \frac{1}{2 \cdot 4} \sum_{\substack{2 \text{ distinct } i,j,k,l \\ \text{one of size 1 the other of size 3}}} A_{ii} B_{kl} + \frac{1}{5} \sum_i A_{ii} B_{ii}.
\end{aligned}$$

□

A naïve way to do calculate $\mathbb{E}[\mathbf{x}^\top \mathbf{A} \mathbf{x} \mathbf{x}^\top \mathbf{B} \mathbf{x}]$ is to iterate through all possible combinations of i, j, k, l and compute the number of unique indices. As calling the `unique` command on the indices is slow, we can reformulate Eq (8) with the use of entrywise multiplication. Define a matrix $\mathbf{C}(i, j)$ as a function of i, j whose entries correspond to the coefficients of the sums in (8) where the indices of $\mathbf{C}(i, j)$ correspond to the indices of \mathbf{B} . An example of the 5×5 case where $i = 2$ and $j = 4$ is given by

$$\mathbf{C}(i, j) = \begin{pmatrix} 1/12 & 1/12 & 1/16 & 1/12 & 1/16 \\ 1/12 & 1/8 & 1/12 & 1/9 & 1/12 \\ 1/16 & 1/12 & 1/12 & 1/12 & 1/16 \\ 1/12 & 1/9 & 1/12 & 1/8 & 1/12 \\ 1/16 & 1/12 & 1/16 & 1/12 & 1/12 \end{pmatrix},$$

and the case where $i = j = 2$ is given by

$$\mathbf{C}(i, j) = \begin{pmatrix} 1/9 & 1/8 & 1/12 & 1/12 & 1/12 \\ 1/8 & 1/5 & 1/8 & 1/8 & 1/8 \\ 1/12 & 1/8 & 1/9 & 1/12 & 1/12 \\ 1/12 & 1/8 & 1/12 & 1/9 & 1/12 \\ 1/12 & 1/8 & 1/12 & 1/12 & 1/9 \end{pmatrix}.$$

If \odot denotes the entrywise product of two matrices, we can express (8) as

$$\begin{aligned} \text{Cov}[\mathbf{x}^\top \mathbf{A} \mathbf{x}, \mathbf{x}^\top \mathbf{B} \mathbf{x}] &= \mathbf{1}^\top \left(\sum_{i,j} A_{ij} (\mathbf{B} \odot \mathbf{C}(i, j)) \right) \mathbf{1} \\ &\quad - \left(\frac{1}{12} \text{tr}(\mathbf{A}) + \frac{1}{4} \mathbf{1}^\top \mathbf{A} \mathbf{1} \right) \left(\frac{1}{12} \text{tr}(\mathbf{B}) + \frac{1}{4} \mathbf{1}^\top \mathbf{B} \mathbf{1} \right). \end{aligned}$$

Now that the computation of the variance and covariance of quadratic polynomials has been covered, we can normalize randomly selected polynomials to obtain a choice of f_0 . Now, we need a way to find an orthogonal h_0 to a randomly selected f_0 .

For the space of polynomials with zero intercept, $\sqrt{\text{Var}[f]}$ is a norm. As such, we can use one step of a modified Gram-Schmidt procedure to obtain an orthogonal polynomial h_0 to a randomly selected polynomial f_0 for purposes of SNR calibration. Now assume f_0 is randomly generated to have unit norm. Let h_0^* also be a randomly generated polynomial with unit norm. Using one step of a modified Gram-Schmidt procedure we set h_0 to be the following polynomial:

$$h_0 := h_0^* - \frac{\langle f_0, h_0^* \rangle}{\|f_0\|} \frac{f_0}{\|f_0\|}.$$

With this construction, $h_0 \perp f_0$ as

$$\begin{aligned} \langle f_0, h_0 \rangle &= \left\langle f_0, h_0^* - \frac{\langle f_0, h_0^* \rangle}{\|f_0\|} \frac{f_0}{\|f_0\|} \right\rangle \\ &= \langle f_0, h_0^* \rangle - \left\langle f_0, \frac{\langle f_0, h_0^* \rangle}{\|f_0\|} \frac{f_0}{\|f_0\|} \right\rangle \\ &= \langle f_0, h_0^* \rangle - \langle f_0, h_0^* \rangle \frac{\langle f_0, f_0 \rangle}{\|f_0\|^2} \\ &= 0. \end{aligned}$$

9.3 Example: Univariate predictor profiles in section 4.2.2 of the main manuscript

The functions used in section 4.2.2 are below:

$$\begin{aligned} f_0(x) &= 0.14953379 x^2 - 0.09938939 x - 0.32320738 \\ h_0^*(x) &= 0.42598510 x^2 - 0.17591160 x + 0.47024360. \end{aligned}$$

The calibrated profiles are below for when $\text{Var}[f] = 6, \text{Var}[\delta], \rho(f, h) = 0.9$ and a convex combination is used:

$$f(x) = 134.0778 f_0(x)$$

$$h(x) = 35.02044 f_0(x) - 5.536481 h_0(x).$$

10 Details regarding the Robot Failures Case Study

In Section 5 of the main article, we apply the proposed control chart and the PCA based control chart on a dataset from Dua and Graff (2017); Camarinha-Matos et al. (1996) which contain force and torque measurements of a robot arm while executing the tasks of grasping an object, transferring it to a new location and ungrasping it.

Visualizations of the robot arm taken from Camarinha-Matos et al. (1996) are provided in Figure 7. Force and torque measurements are collected along three axes every 315 ms for 4.725s under various task completion and failure scenarios. Table 6 provides a summary of the types of task completion and failure scenarios. Figure 8 provides a visualization of the various failure scenarios in comparison the the normal operating scenarios for the LP-1 Task where a robot arm approaches and grasps an object.

Task ID	Failures in . . .	Class	Sample Size
LP-1	approach-grasp	normal	21
		collision	17
		front collision	16
		obstruction	34
LP-2	transfer of a part (system behavior)	normal	20
		front collision	6
		back collision	7
		collision to the right	5
LP-3	transferred location (handled part)	collision to the left	9
		ok	20
		slightly moved	15
		moved	9
LP-4	approach-ungrasp	lost	3
		normal	24
		collision	72
LP-5	motion with part	obstruction	21
		normal	44
		bottom collision	26
		bottom obstruction	21
		collision in part	47
		collision in tool	26

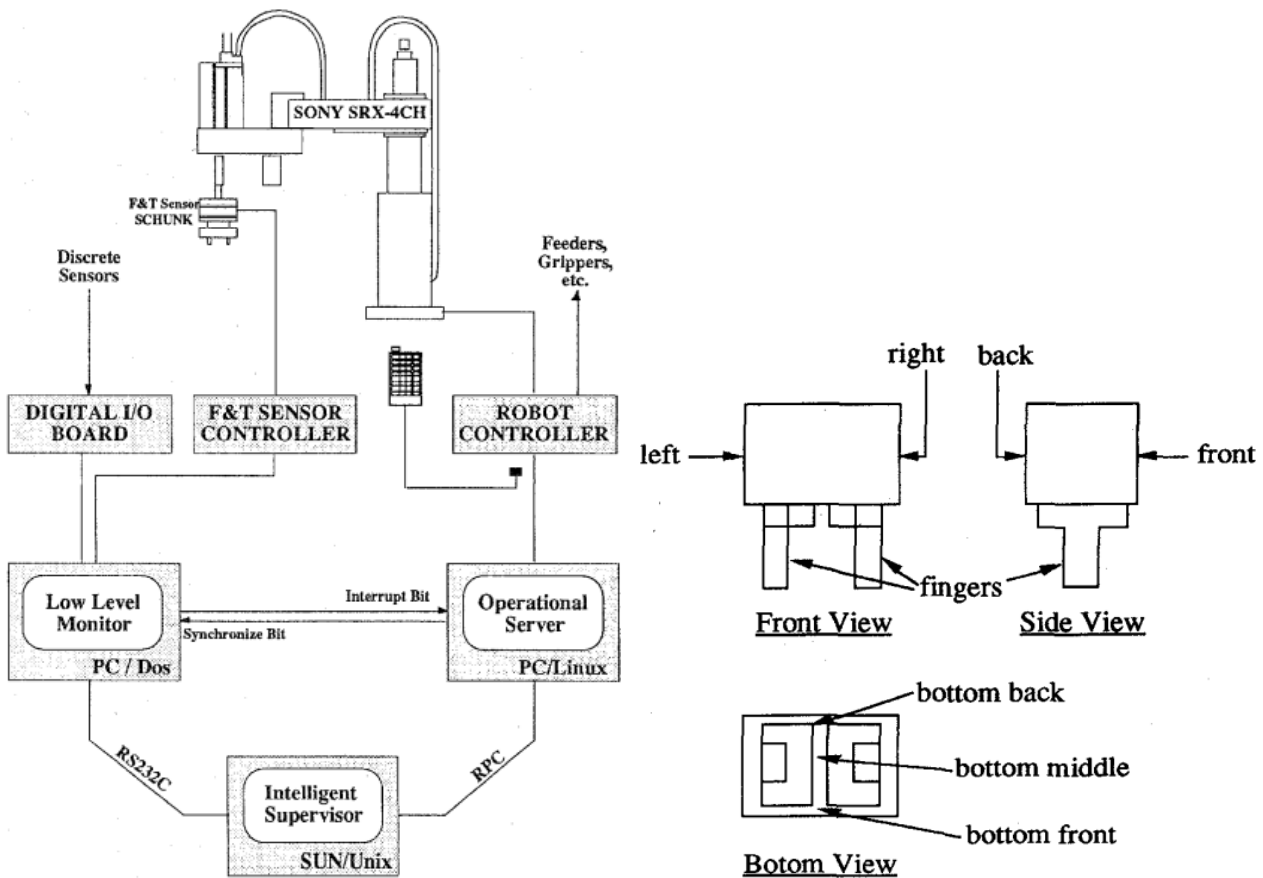
Table 6: A summary of the tasks in the Robot Failures dataset from (Camarinha-Matos et al. 1996) which can be found on Dua and Graff (2017).

We use the data from the LP-1 Task ID where the robot arm approaches and grasps an object as all other tasks seemed to have multiple ways to be IC. Of the 21 normal profiles

in LP-1 we remove three profiles as their residuals after mean (profile) centering are nearly perfectly correlated.

Observe in Figure 8, if the six sensor readings for a single profile across the 4.725s window are stacked in a single vector, the amount of variability of the in-control function is quite large especially in comparison to the variability around the in-control function. That is to say, for this dataset $\text{Var}[f] \gg \sigma^2$. Despite the “small” sample size of $n = 90$ for each profile in this dataset and the small values of m and w used in the simulation study, the FAR of the EPCC is still quite low due to the large value of $\text{Var}[f]/\sigma^2$.

Regarding the control chart’s out-of-control performance, notice the correlation structure between the IC and OOC profiles in Figure 9 has a clear 2×2 block structure where the upper left block is the correlation of two IC profiles. The off diagonal blocks are correlations of an IC profile with an OOC profile, and the lower right block corresponds to the correlation between two OOC profiles. Compare Figure 9 in this response to Figure 1 in the main manuscript and observe the correlation matrices in Figure 9 deviates further from Figure 1a from the main manuscript than Figure 1b from the main manuscript does in all but the upper left block. This should suggest that our control chart should have good out-of-control performance, which is supported by the simulation study in the main manuscript.



(a) Assembly cell integrating infrastructure (B-LEARN(b) Regions of a gripper that may be involved in a failure project)

Figure 7: Visualizations of the Robot Arm taken from Camarinha-Matos et al. (1996).

25th & 75th percentiles of Robot Arm Sensor Readings for Approach/Grasp Task

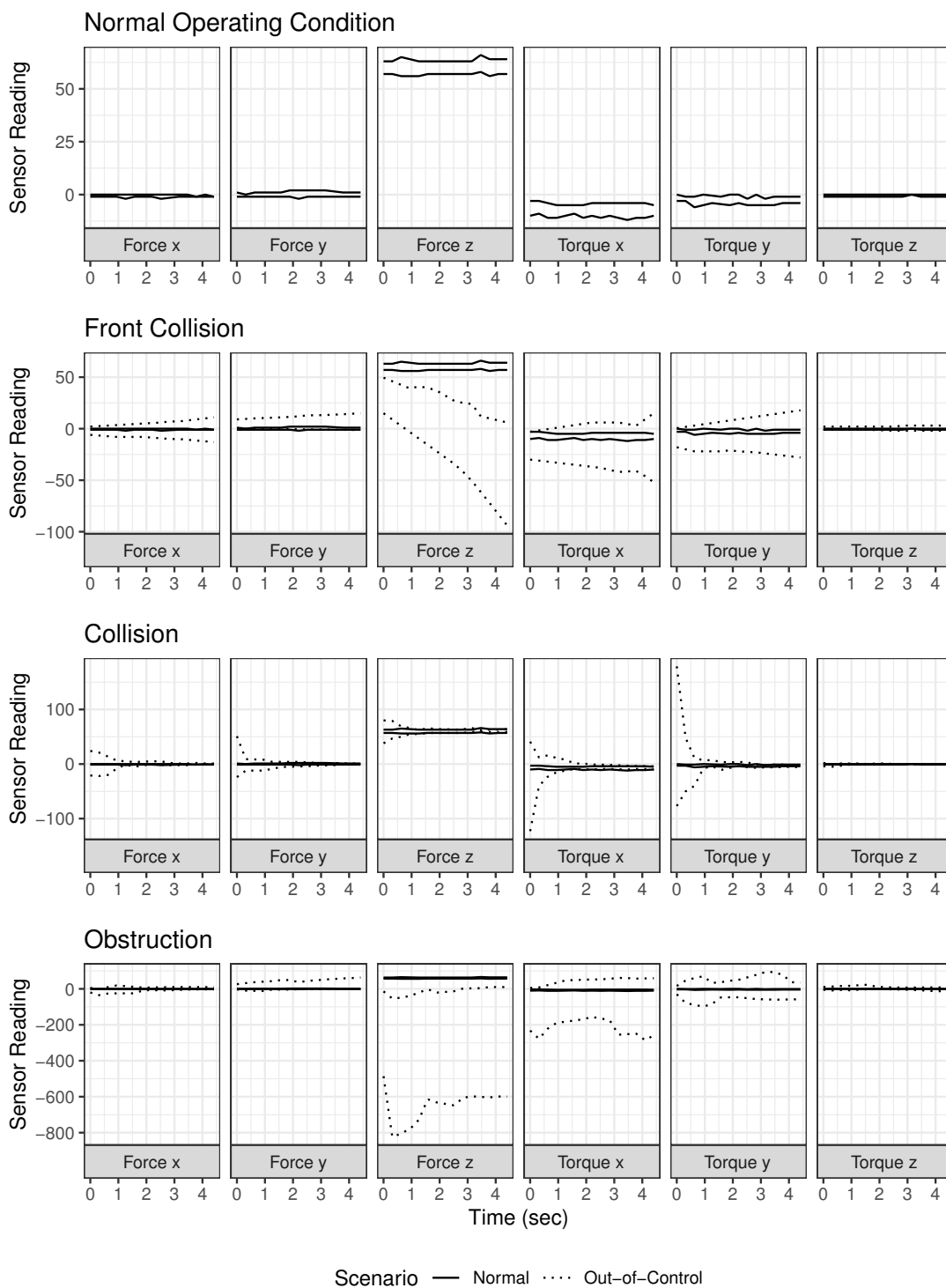


Figure 8: A comparison of the sensor readings between in-control and out-of-control robot arm operation. For each out-of-control scenario, we plot fitted percentiles of the observed sensor readings across time of execution.

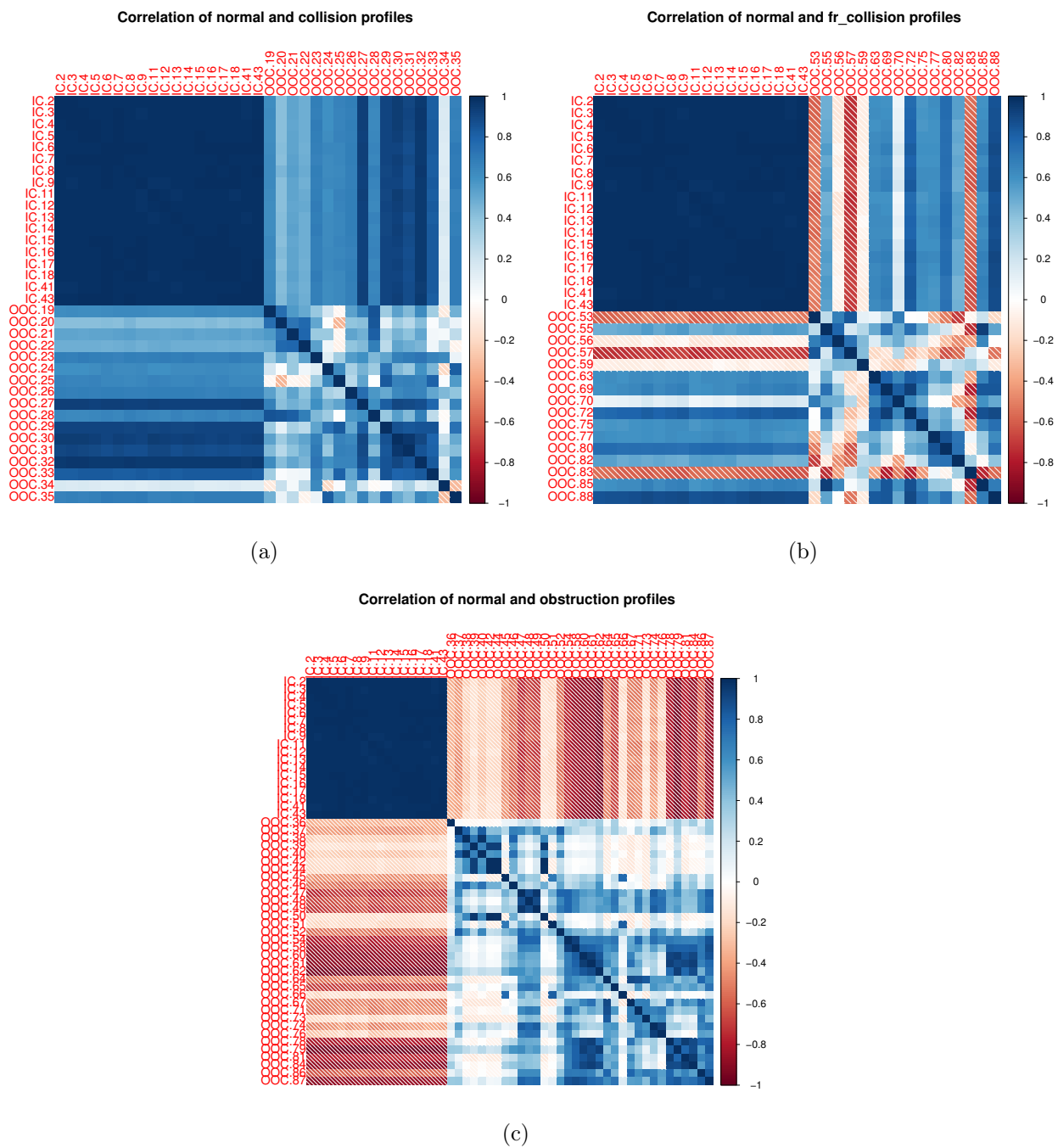


Figure 9: The sample correlation between profiles in the Robot Failures Dataset. Rows/-columns labeled with an ‘IC’ (‘OOC’) are the in-control (out-of-control) profiles where sensor readings are taken under normal (abnormal) operating conditions.

References

- Ackleh, A. S., E. J. Allen, R. B. Kearfott, and P. Seshaiyer (2009, July). *Classical and modern numerical analysis*. Chapman and Hall/CRC.
- Camarinha-Matos, L., L. Lopes, and J. Barata (1996). Integration and learning in supervision of flexible assembly systems. *IEEE Transactions on Robotics and Automation* 12(2), 202–219.
- Dua, D. and C. Graff (2017). UCI machine learning repository.
- Iguchi, T., A. F. Barrientos, E. Chicken, and D. Sinha (2021). Nonlinear profile monitoring with single index models. *Quality and Reliability Engineering International* 37(7), 3004–3017.
- Iguchi, T., D. G. Mixon, J. Peterson, and S. Villar (2017). Probably certifiably correct k -means clustering. *Math. Program., Ser. A* 165, 605–642.
- Li, C. I., J. N. Pan, and C. H. Liao (2019). Monitoring nonlinear profile data using support vector regression method. *Quality and Reliability Engineering International* 35(1), 127–135.
- Qiu, P., C. Zou, and Z. Wang (2010). Nonparametric profile monitoring by mixed effects modeling. *Technometrics* 52(3), 265–277.
- Williams, J. D., W. H. Woodall, and J. B. Birch (2007, Dec). Statistical monitoring of nonlinear product and process quality profiles. *Quality and Reliability Engineering International* 23(8), 925–941.
- Zou, C., F. Tsung, and Z. Wang (2008). Monitoring profiles based on nonparametric regression methods. *Technometrics* 50(4), 512–526.